Available online at www.sciencedirect.com
ScienceDirect
Mathematics and Computers in Simulation 212 (2023) 138–158
MATHEMATICS AND COMPUTERS IN SIMULATION
www.elsevier.com/locate/matcom

Original articles

A finite element approximation to a viscoelastic Euler–Bernoulli beam with internal damping

Yiqun Li, Hong Wang*

Department of Mathematics, University of South Carolina, Columbia, SC 29208, USA

Received 30 January 2023; received in revised form 8 April 2023; accepted 25 April 2023
Available online 3 May 2023

Abstract

We analyze a finite element approximation to a viscoelastic Euler–Bernoulli beam with internal damping that undergoes vibrations under external excitation. We prove the wellposedness of the problem and regularity estimates of the exact solution to the model. We then utilize these results to prove an optimal-order error estimate of the numerical approximation assuming only the regularity of the data of the model but not that of the exact solution. Because the model exhibits its salient features that are different from those of conventional elastic Euler–Bernoulli beams, a new estimate technique is used in the analysis. We finally carry out numerical experiments to substantiate the error estimate and to investigate the dynamic response of the viscoelastic Euler–Bernoulli beam, in comparison with the conventional Euler–Bernoulli beam.

Keywords: Viscoelastic Euler–Bernoulli beam; Variable-order time fractional PDE; Regularity estimate; Finite element approximation; Error estimate

1. Introduction

Various materials widely applied in mechanical and biological systems are viscoelastic, which exhibit viscous behavior of newtonian fluid as well as elastic characteristics of solids through simultaneous dissipation and storage of mechanical energy [2,4,6,11,18]. Power-law rheology is a constitutive behavior widely observed in a diverse range of viscoelastic materials which demonstrate hereditary phenomenon with long memory effects, e.g., anomalous power-law relaxation/creep [2,4,6,9,30]. Conventional rheological viscoelastic models progressively combine several Hookean springs and Newtonian dashpots to characterize elastic and viscous properties of the viscoelastic materials and to catch the complex hereditary behavior of the viscoelastic materials. Nevertheless, these well-known integer-order models, which are fundamentally multi-exponential decaying functions, merely describe a truncated power-law relaxation and do not provide a satisfactory quantitative behavior of real materials [2,4,9,11].

Motivated by the power-law behavior of viscoelastic materials, fractional calculus is considered as a natural candidate to mathematically model the experimentally observed power-law dynamics of the viscoelastic materials.

* Corresponding author.
E-mail addresses: yiqunl@email.sc.edu (Y. Li), hwang@math.sc.edu (H. Wang).

https://doi.org/10.1016/j.matcom.2023.04.031
0378-4754/

A Scott-Blair element with the power-law relaxation modulus and the assumptions that the material is quiescent for $t < 0$ and $\varepsilon(0) = 0$

$$\begin{aligned} &\sigma(t) = E_\alpha\, \partial_t^\alpha \varepsilon(t) = \frac{E_\alpha}{\Gamma(1-\alpha)} \int_0^t \frac{\varepsilon'(s)}{(t-s)^\alpha} ds, \quad 0 < \alpha < 1, \\ &\partial_t^\alpha v(t) := {}_0I_t^{1-\alpha} v'(t), \quad {}_0I_t^\alpha v(t) := \frac{1}{\Gamma(\alpha)} \int_0^t \frac{v(s)}{(t-s)^{1-\alpha}} ds \end{aligned} \tag{1.1}$$

provides a constitutive interpolation between Hookean springs as $\alpha \to 0$ and Newtonian dashpots as $\alpha \to 1$, and has been widely used to model strain–stress relation for viscoelastic material as it correctly catches the power-law behavior of viscoelastic materials [4,18,23,26,31]. Here σ and ε represent the stress and strain of the material, respectively, the fractional operator ∂_t^α is the Caputo fractional differential operator defined in (1.1) [10,31] and E_α is a material dependent constant.

Despite the extensive applications of the fractional viscoelastic models, various experiments show that many viscoelastic materials demonstrate variable-order power-law behaviors [4,32]. For instance, as viscoelastic systems vibrate due to long-term cyclic loads, they endure micro-structures changes which may lead to the change of material properties. These processes may in turn cause mechanical structural damages, which further propagate to macro scales that eventually result in material failure. Such multi-scale physics change the characteristic fractal dimensions of the microstructure, which in turn causes the change of the fractional order in the strain–stress relation [29]. A variable-order stress–strain relation better describes the heterogeneous multi-scale material properties of the viscoelastic materials, leading to variable-order fractional PDEs [13,38,39,47,52].

In comparison with the comprehensive studies for the fractional diffusion PDEs [19,20,22,37,43,46,48], numerical approximations for the model (2.6)–(2.7) (cf. Section 2) are rare in the literature due to, e.g., lack of high-order regularity estimates of the solution. To compensate for this gap, we firstly follow the modeling procedure to present the derivation of this problem and prove the well-posedness and the solution regularity of the proposed model. We then accordingly prove an optimal-order error estimates of the finite element scheme to the problem assuming only the regularity of the data of the model but not that of the exact solution. Because the model exhibits its salient features that are different from those of conventional elastic Euler–Bernoulli models, a new estimate technique is used in the analysis. The rest of the paper is organized as follows. In Section 2, we develop the governing PDE for the viscoelastic Euler–Bernoulli beam and introduce notations and preliminaries. In Section 3, we prove the well-posedness of the problem and the regularity of its solutions. In Section 4, we develop a fully-discretized finite element scheme to the model and then prove its optimal convergence rate. In Section 5, we perform some numerical experiments to verify the numerical analysis and to investigate the dynamic response of the viscoelastic Euler–Bernoulli beam, in comparison with the conventional Euler–Bernoulli beam.

2. Model and preliminaries

2.1. A viscoelastic Euler–Bernoulli beam

We consider the small transverse vibrations of a viscoelastic beam under the hypotheses: (i) The beam has a straight centroidal axis, length l, cross sectional area A, and mass density ρ (see Fig. 1). (ii) All the loadings and supports are symmetric about the xz plane. (iii) Cross sectional planes that are perpendicular to the centroidal axis of the undeformed beam remain planar after deformation and are perpendicular to the deflection curve of the deformed beam. The strains acting in the cross section are only due to the bending kinematics and the beam undergoes purely planar flexural vibrations. This reduces the problem of beam vibration to the study of the motion of the deflection curve and reduces the problem to one space dimension.

Given the distributed transverse excitation $q(x,t)$, let $w(x,t)$ be the deflection of the centroidal beam axis, Let $M(x,t)$ and $V(x,t)$ be the internal bending moment and shear force, respectively. We demonstrate the Euler–Bernoulli beam model in Fig. 1 which is simply supported by the edges. A standard balance equation is as follows [5,17,33,34,41]

$$\rho A \partial_t^2 w + \partial_x^2 M = q(x,t). \tag{2.1}$$

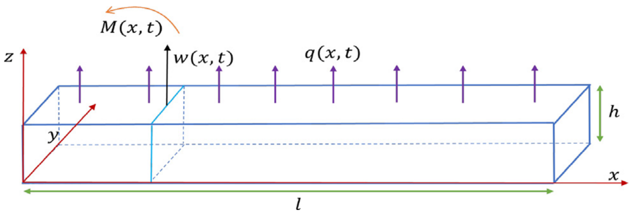

Fig. 1. Transverse vibration of a viscoelastic simply-supported Euler–Bernoulli beam with length l and thickness h under a distributed transverse load $q(x,t)$.

Put the variable-order constitutive relation [32,38] and the kinetic equation $\varepsilon_{xx} = -z\partial_x^2 w$ obtained under the Euler–Bernoulli beam assumptions [5,17,33,34] to express the stress in terms of the variable-order time-fractional derivative of the beam deflection to describe the variable power-law behavior of the viscoelastic material as follows

$$\sigma_{xx}(x,z,t) = E_\alpha\, \partial_t^{\alpha(t)} \varepsilon_{xx}(x,z,t) = -E_\alpha z\, \partial_t^{\alpha(t)} \partial_x^2 w(x,t), \tag{2.2}$$

where the variable-order fractional differential operator $\partial_t^{\alpha(t)}$ is defined by [25,36]

$$\partial_t^{\alpha(t)} g(t) := {}_0I_t^{1-\alpha(t)} \dot{g}(t), \quad {}_0I_t^{\alpha(t)} g(t) := \int_0^t \frac{g(s)}{\Gamma(\alpha(s))(t-s)^{1-\alpha(s)}} ds. \tag{2.3}$$

The net bending moment $M(x,t)$ is evaluated as

$$M(x,t) = -\int_A z\sigma_{xx}(x,z,t) dA = E_\alpha I \partial_t^{\alpha(t)} \partial_x^2 w, \tag{2.4}$$

where $I = \int_A z^2 dA$ is the cross-sectional moment of inertial about the y axis.

We follow [3,7,15] to account for the internal damping effect of the energy dissipated by the inter-particle friction internal to the structure during vibrations, by the time rate of change of the (elastic component) of the normal strain. Hence, Eq. (2.4) is augmented to be

$$M(x,t) = E_\alpha I \partial_t^{\alpha(t)} \partial_x^2 w + E_d I \partial_t \partial_x^2 w, \tag{2.5}$$

where $E_d > 0$ is the internal damping coefficient. We incorporate Eq. (2.5) into Eq. (2.1) to derive a viscoelastic Euler–Bernoulli beam model including internal damping effect

$$\partial_t^2 w + K \partial_t \partial_x^4 w + K_\alpha \partial_t^{\alpha(t)} \partial_x^4 w = q/(\rho A), \quad (x,t) \in (0,l) \times (0,T]. \tag{2.6}$$

Here $K := E_d I/(\rho A)$, $K_\alpha := E_\alpha I/(\rho A)$. We assume the beam to be simply supported, leading to the initial and boundary conditions

$$\begin{array}{lll} w(x,0) = w_0(x), & \partial_t w(x,0) = \check{w}_0(x), & x \in [0,l], \\ w(0,t) = w(l,t) = 0, & M(0,t) = M(l,t) = 0, & t \in [0,T]. \end{array} \tag{2.7}$$

We express Eq. (2.6) in terms of $u = \partial_t w$ as follows

$$\partial_t u + K \partial_x^4 u + K_\alpha\, {}_0I_t^{1-\alpha(t)} \partial_x^4 u = q/(\rho A), \quad (x,t) \in (0,l) \times (0,T]. \tag{2.8}$$

Utilize the uniqueness of the solution to the homogeneous second-kind Volterra integral equation to express the boundary conditions (2.7) as boundary conditions in terms of u as follows

$$\begin{array}{ll} u(x,0) = \check{w}_0(x), & x \in [0,l], \\ u(0,t) = u(l,t) = \partial_x^2 u(0,t) = \partial_x^2 u(l,t) = 0, & t \in [0,T]. \end{array} \tag{2.9}$$

2.2. Preliminaries

Let $L^p(\mathcal{I})$, with $1 \le p \le \infty$ and $\mathcal{I}$ be a bounded interval, be the Banach space of pth power Lebesgue integrable functions on $\mathcal{I}$. Let $W^{m,p}(\mathcal{I})$, with $m \in \mathbb{N}$, be the sobolev space of m time weakly differentiable functions in $L^p(\mathcal{I})$, and let $H^m(\mathcal{I}) = W^{m,2}(\mathcal{I})$. Let $C^m(\bar{\mathcal{I}})$ be the Banach space of m time continuously differentiable functions on the closed interval $\bar{\mathcal{I}}$ and $H_0^m(\mathcal{I})$ be the completion of $C_0^\infty(\mathcal{I})$, the space of infinitely differentiable functions with compact support functions in $\mathcal{I}$, with respect to the norm in $H^m(\mathcal{I})$. For a non-integer s, the fractional Sobolev space $H^s(\mathcal{I})$ is defined by interpolation. All the spaces are equipped with standard norms [1].

For a Banach space $\mathcal{X}$ equipped with the norm $\|\cdot\|_{\mathcal{X}}$, let $C^m([0,T];\mathcal{X})$ be the space of functions with continuous derivatives up to order m on $[0,T]$ belonging to $\mathcal{X}$ equipped with the norm

$$C^m([0,T],\mathcal{X}) := \left\{g : [0,T] \to \mathcal{X} : \ \|\partial_t^l g(\cdot,t)\|_{\mathcal{X}} \in C^l[0,T], \quad l = 0,1,\ldots,m\right\},$$
$$\|g\|_{C^m([0,T],\mathcal{X})} := \max_{0\le l\le m} \max_{t\in[0,T]} \|\partial_t^l g(\cdot,t)\|_{\mathcal{X}}.$$

The eigenfunctions $\{\phi_i\}_{i=1}^\infty$ of $-\partial_x^2$ on $x \in (0,l)$ form an orthonormal basis in $L^2(0,l)$ and the corresponding eigenvalues $\{\lambda_i\}_{i=1}^\infty$ form a positive nondecreasing sequence which tend to infinity [12]. For $s \ge 0$ we use the theory of sectorial operators to define the fractional Sobolev spaces [24,35,42]

$$\check{H}^s(0,l) := \left\{v \in L^2(0,l) : |v|_{\check{H}^s}^2 = \sum_{i=1}^\infty \lambda_i^s (v,\phi_i)^2 < \infty\right\}$$

equipped with the norm $\|v\|_{\check{H}^s} = (\|v\|_{L^2}^2 + |v|_{\check{H}^s}^2)^{1/2}$. $\check{H}^s(0,l)$ is the subspace of the fractional sobolev space $H^s(0,l)$ and the seminorms $|v|_{\check{H}^s}$ and $|v|_{H^s}$ are equivalent on $\check{H}^s(0,l)$. In particular, $\check{H}^0(0,l) = L^2(0,l)$ and $\check{H}^2(0,l) = H^2(0,l) \cap H_0^1(0,l)$.

In the remaining paper, we use Q, Q_i, M_i to denote positive constants and Q may assume different values at different occurrences. We drop the subscript L^2 in $(\cdot,\cdot)_{L^2}$ and $\|\cdot\|_{L^2}$ and the domain $(0,l)$ in the Sobolev spaces and norms when no confusion occurs.

3. Regularity estimates of the exact solution

3.1. Analysis of a variable-order ordinary differential equation

We consider the wellposedness and solution regularity of the following variable-order fractional ordinary differential equation motivated by (3.3)

$$y'(t) + K\lambda^2 y(t) + K_\alpha \lambda^2 \, {}_0I_t^{1-\alpha(t)} y(t) = g(t), \quad t \in (0,T], \quad y(0) = \hat{y}_0. \tag{3.1}$$

Here λ, $g(t)$ and $\hat{y}_0$ are given data.

Theorem 3.1. *If $g \in L^2(0,T)$ and $0 \le \alpha(t) < \alpha^* < 1$ for some upper bound α^*, then the variable-order fractional ordinary differential equation (3.1) has a unique solution $y \in H^1(0,T)$ and*

$$\|y\|_{L^2(0,T)} \le Q(\lambda^{-2}\|g\|_{L^2(0,T)} + \lambda^{-1}\left|\hat{y}_0\right|), \ \ \|y'\|_{L^2(0,T)} \le Q(\|g\|_{L^2(0,T)} + \lambda\left|\hat{y}_0\right|). \tag{3.2}$$

Here the positive constant $Q = Q(K, K_\alpha, \alpha^*, T)$.

Proof. We integrate (3.1) multiplied by $e^{K\lambda^2 t}$ to obtain a Volterra integral equation of the second kind in terms of $y(t)$

$$\begin{aligned} y(t) &= -K_\alpha\lambda^2 \int_0^t e^{-K\lambda^2(t-s)} {}_0I_s^{1-\alpha(s)} y(s)\,ds + \int_0^t e^{-K\lambda^2(t-s)} g(s)ds + e^{-K\lambda^2 t}\hat{y}_0 \\ &= -K_\alpha\lambda^2 e^{-K\lambda^2 t} * {}_0I_t^{1-\alpha(t)} y(t) + e^{-K\lambda^2 t} * g(t) + e^{-K\lambda^2 t}\hat{y}_0. \end{aligned} \tag{3.3}$$

Here $*$ represents the symbol of convolution on $[0,t]$ as follows

$$g_1(t) * g_2(t) := \int_0^t g_1(s) g_2(t-s) ds.$$

To prove the wellposedness of the problem (3.3), let $\mathcal{X} := L^2(0,T)$ equipped with the norm $\|g\|_{\mathcal{X},\gamma} := \|e^{-\gamma t} g\|_{L^2(0,T)}$ for some fixed $\gamma \ge 0$. For each $y \in \mathcal{X}$, let $z := \mathcal{M}y$ be the solution of

$$z(t) = -K_\alpha\lambda^2 e^{-K\lambda^2 t} * {}_0I_t^{1-\alpha(t)} y(t) + e^{-K\lambda^2 t} * g(t) + e^{-K\lambda^2 t}\hat{y}_0, \tag{3.4}$$

and the last two terms on its right hand side can be bounded by employing Young's inequality

$$\begin{aligned}&\big\|e^{-K\lambda^2 t} * g(t)\big\|_{L^2(0,T)} \le \big\|e^{-K\lambda^2 t}\big\|_{L^1(0,T)}\|g\|_{L^2(0,T)} \le Q\lambda^{-2}\|g\|_{L^2(0,T)},\\ &\big\|e^{-K\lambda^2 t}\hat{y}_0\big\|_{L^2(0,T)} \le Q\lambda^{-1}\left|\hat{y}_0\right|.\end{aligned} \tag{3.5}$$

We utilize the following estimates

$$\begin{aligned}&(t-s)^{-\alpha(s)} = (t-s)^{-\alpha^*}(t-s)^{\alpha^*-\alpha(s)} \le \max\{1,T\}(t-s)^{-\alpha^*},\\ &\int_0^T e^{-\gamma t}t^{-\alpha^*}dt \le \gamma^{\alpha^*-1}\int_0^\infty e^{-s}s^{-\alpha^*}ds = \gamma^{\alpha^*-1}\Gamma(1-\alpha^*),\end{aligned} \tag{3.6}$$

the definition (2.3) and Young's inequality to bound the first term on the right hand side of (3.4) by

$$\begin{aligned}\big\|K_\alpha\lambda^2 e^{-K\lambda^2 t} * {}_0I_t^{1-\alpha(t)}y\big\|_{\mathcal{X},\gamma} &= \big\|K_\alpha\lambda^2 e^{-(K\lambda^2+\gamma)t} * \big(e^{-\gamma t}{}_0I_t^{1-\alpha(t)}y\big)\big\|_{L^2(0,T)}\\ &\le Q\lambda^2\big\|e^{-(K\lambda^2+\gamma)t}\big\|_{L^1(0,T)}\big\|e^{-\gamma t}{}_0I_t^{1-\alpha(t)}y\big\|_{L^2(0,T)}\\ &\le Q\left\|\int_0^t \frac{e^{-\gamma(t-s)}}{\Gamma(1-\alpha(s))(t-s)^{\alpha(s)}}e^{-\gamma s}y(s)ds\right\|_{L^2(0,T)}\\ &\le Q\left\|\int_0^t \frac{e^{-\gamma(t-s)}}{(t-s)^{\alpha^*}}e^{-\gamma s}|y(s)|ds\right\|_{L^2(0,T)}\\ &\le Q\|e^{-\gamma t}t^{-\alpha^*}\|_{L^1(0,T)}\big\|e^{-\gamma t}y\big\|_{L^2(0,T)}\\ &\le Q\gamma^{\alpha^*-1}\big\|e^{-\gamma t}y\big\|_{L^2(0,T)},\end{aligned} \tag{3.7}$$

which, together with the estimates (3.5), implies that the operator $\mathcal{M}:\mathcal{X}\to\mathcal{X}$ is well-defined and

$$\|z\|_{\mathcal{X},\gamma} \le Q(\lambda^{-2}\|g\|_{L^2(0,T)} + \lambda^{-1}\left|\hat{y}_0\right|) + Q\gamma^{\alpha^*-1}\big\|y\big\|_{\mathcal{X},\gamma}. \tag{3.8}$$

Furthermore, for $y_i \in \mathcal{X}$ and $z_i := \mathcal{M}y_i$ for $i = 1, 2$, we have

$$\|z_1 - z_2\|_{\mathcal{X},\gamma} \le Q\gamma^{\alpha^*-1}\big\|y_1 - y_2\big\|_{\mathcal{X},\gamma}. \tag{3.9}$$

Thus, $\mathcal{M}$ is a contraction mapping from $\mathcal{X}\to\mathcal{X}$ provided that γ is chosen such that $Q\gamma^{\alpha^*-1} < 1$, which implies the integral equation (3.3) (and thus the differential equation (3.1)) admits a unique solution in $L^2(0,T)$. Let $y = \mathcal{M}y$ be the fixed point, then (3.8) becomes

$$\|y\|_{\mathcal{X},\gamma} \le Q(\lambda^{-2}\|g\|_{L^2(0,T)} + \lambda^{-1}\left|\hat{y}_0\right|) + Q\gamma^{\alpha^*-1}\big\|y\big\|_{\mathcal{X},\gamma}, \tag{3.10}$$

choosing sufficiently large γ in (3.10) yields that

$$\|e^{-\gamma t}y\|_{L^2(0,T)} \le Q(\lambda^{-2}\|g\|_{L^2(0,T)} + \lambda^{-1}\left|\hat{y}_0\right|). \tag{3.11}$$

Thus we prove the first estimate in (3.2) by (3.11).

To bound y', we differentiate (3.3) with respect to t to obtain

$$\begin{aligned}y'(t) = &-K_\alpha\lambda^2{}_0I_t^{1-\alpha(t)}y(t) + K_\alpha K\lambda^4 e^{-K\lambda^2 t} * {}_0I_t^{1-\alpha(t)}y(t)\\ &-K\lambda^2 e^{-K\lambda^2 t} * g(t) + g(t) - K\lambda^2 e^{-K\lambda^2 t}\hat{y}_0.\end{aligned} \tag{3.12}$$

We apply the preceding estimates (3.6)–(3.7) and Young's convolution inequality to bound

$$\begin{aligned}\big\|K_\alpha\lambda^2{}_0I_t^{1-\alpha(t)}y(t)\big\|_{L^2(0,T)} &\le Q\lambda^2\left\|\int_0^t |y(s)|\,(t-s)^{-\alpha^*}ds\right\|_{L^2(0,T)}\\ &\le Q\lambda^2\|t^{-\alpha^*}\|_{L^1(0,T)}\|y\|_{L^2(0,T)} \le Q\lambda^2\|y\|_{L^2(0,T)},\\ \big\|K_\alpha K\lambda^4 e^{-K\lambda^2 t} * {}_0I_t^{1-\alpha(t)}y(t)\big\|_{L^2(0,T)} &\le Q\lambda^4\big\|e^{-K\lambda^2 t}\big\|_{L^1(0,T)}\big\|{}_0I_t^{1-\alpha(t)}y\big\|_{L^2(0,T)}\\ &\le Q\lambda^2\|t^{-\alpha^*}\|_{L^1(0,T)}\|y\|_{L^2(0,T)} \le Q\lambda^2\|y\|_{L^2(0,T)},\end{aligned} \tag{3.13}$$

and then we combine (3.12) with the above estimates, the estimates in (3.5) as well as the first estimate in (3.2) to arrive at

$$\|y'\|_{L^2(0,T)} \le Q(\lambda^2\|y\|_{L^2(0,T)} + \|g\|_{L^2(0,T)} + \lambda\left|\hat{y}_0\right|) \le Q(\|g\|_{L^2(0,T)} + \lambda\left|\hat{y}_0\right|), \tag{3.14}$$

which completes the proof.

Remark 3.1. In the proof of Theorem 3.1, we require the variable order α is bounded above by α^* which is strictly away from 1. This constraint is crucial to ensure that the mapping (3.8) is a contraction, which in turn guarantees the uniqueness of the solution to the problem (3.1). The resulting positive constant Q for both estimates in (3.2) depends on α^*, T, K_α and K by the estimates (3.5)–(3.7) and (3.13)–(3.14).

Theorem 3.2. *Suppose $0 \le \alpha(t) < \alpha^* < 1$ for some upper bound α^*, $\alpha \in C^1[0,T]$ and $g \in H^1(0,T)$, then the following weighted stability estimate holds*

$$\left\|t^{\frac{\alpha(0)}{2}} y''\right\|_{L^2(0,T)} \le Q(\lambda^2\|g\|_{L^2(0,T)} + \|g\|_{H^1(0,T)} + \lambda^3\left|\hat{y}_0\right|) \tag{3.15}$$

with $Q = Q(K, K_\alpha, \alpha^*, \|\alpha\|_{C^1[0,T]}, T)$.

Proof. To derive an stability estimate for y'', we differentiate (3.3) twice with respect to t to obtain

$$\begin{aligned} y''(t) = &-K_\alpha\lambda^2\left({}_0I_t^{1-\alpha(t)}y\right)_t + K_\alpha K\lambda^4\,{}_0I_t^{1-\alpha(t)}y(t)\\ &-K_\alpha K^2\lambda^6 e^{-K\lambda^2 t} * {}_0I_t^{1-\alpha(t)}y(t) - K\lambda^2 g(t)\\ &\quad+K^2\lambda^4 e^{-K\lambda^2 t} * g(t) + g'(t) + K^2\lambda^4 e^{-K\lambda^2 t}\hat{y}_0. \end{aligned} \tag{3.16}$$

To evaluate the first term on the right hand side of (3.16), we first integrate y by parts to get

$$\begin{aligned} {}_0I_t^{1-\alpha(t)}y &= -\frac{1}{1-\alpha(t)}\int_0^t \frac{y(s)d(t-s)^{1-\alpha(t)}}{\Gamma(1-\alpha(s))(t-s)^{\alpha(s)-\alpha(t)}} := \frac{G_y(t)}{1-\alpha(t)},\\ G_y(t) &:= \frac{\hat{y}_0 t^{1-\alpha(0)}}{\Gamma(1-\alpha(0))} + \int_0^t (t-s)^{1-\alpha(s)}\left[\frac{\Gamma'(1-\alpha(s))\alpha'(s)y(s)}{\Gamma(1-\alpha(s))^2}\right.\\ &\quad\left.+\frac{y'(s)}{\Gamma(1-\alpha(s))} - \frac{y(s)}{\Gamma(1-\alpha(s))}\left(\alpha'(s)\ln(t-s) + \frac{\alpha(t)-\alpha(s)}{t-s}\right)\right]ds. \end{aligned} \tag{3.17}$$

Thus we get

$$\left({}_0I_t^{1-\alpha(t)}y\right)_t = \frac{G_y'(t)}{1-\alpha(t)} + \frac{G_y(t)\alpha'(t)}{(1-\alpha(t))^2} \tag{3.18}$$

with

$$\begin{aligned} G_y'(t) = &\frac{\hat{y}_0 t^{-\alpha(0)}}{\Gamma(-\alpha(0))} + {}_0I_t^{1-\alpha(t)}\Bigg((1-\alpha(s))y'(s) - (1-\alpha(s))\alpha'(s)y(s)\\ &\times\left[\ln(t-s) - \frac{\Gamma'(1-\alpha(s))}{\Gamma(1-\alpha(s))}\right] - y(s)\left[\alpha'(s) + \alpha'(t) - \frac{\alpha(s)(\alpha(t)-\alpha(s))}{t-s}\right]\Bigg). \end{aligned}$$

We combine the estimate

$$\frac{|\ln(t-s)|}{(t-s)^{\alpha(s)}} \le Q\frac{|\ln(t-s)|}{(t-s)^{\alpha^*}} = Q\frac{|\ln(t-s)|\,(t-s)^{(1-\alpha*)/2}}{(t-s)^{(1+\alpha*)/2}} \le \frac{Q}{(t-s)^{(1+\alpha*)/2}} \tag{3.19}$$

with the preceding estimates (3.2) to bound

$$\begin{aligned} \left\|{}_0I_t^{1-\alpha(t)}y(s)\ln(t-s)\right\|_{L^2(0,T)} &\le Q\left\|\int_0^t \frac{|y(s)\ln(t-s)|}{(t-s)^{\alpha(s)}}ds\right\|_{L^2(0,T)}\\ &\le Q\|y\|_{L^2(0,T)}\left\|t^{-(1+\alpha*)/2}\right\|_{L^1(0,T)} \le Q\|y\|_{L^2(0,T)},\\ \left\|{}_0I_t^{1-\alpha(t)}y'(s)\right\|_{L^2(0,T)} &\le Q\|y'\|_{L^2(0,T)}\left\|t^{-\alpha*}\right\|_{L^1(0,T)} \le Q\|y'\|_{L^2(0,T)}. \end{aligned} \tag{3.20}$$

We combine (3.17)–(3.18) with the estimates in (3.20) to bound the first term on the right hand side of (3.16)

$$\begin{aligned}\left\| K_\alpha \lambda^2 t^{\frac{\alpha(0)}{2}} \left({}_0I_t^{1-\alpha(t)} y\right)_t \right\|_{L^2(0,T)} &\le Q(\lambda^2 \left|\hat{y}_0\right| + \lambda^2 \|y\|_{L^2(0,T)} + \lambda^2 \|y'\|_{L^2(0,T)}) \\ &\le Q(\lambda^2 \|g\|_{L^2} + \lambda^3 \left|\hat{y}_0\right|).\end{aligned} \tag{3.21}$$

We apply the estimates in (3.5) and Theorem 3.1 to bound the remaining terms in (3.16)

$$\begin{aligned}\left\| K^2 \lambda^4 e^{-K\lambda^2 t} * g(t) \right\|_{L^2(0,T)} &\le Q\lambda^4 \left\| e^{-K\lambda^2 t} \right\|_{L^1(0,T)} \|g\|_{L^2(0,T)} \\ &\le Q\lambda^2 \|g\|_{L^2(0,T)}, \\ \left\| K_\alpha K^2 \lambda^6 e^{-K\lambda^2 t} * {}_0I_t^{1-\alpha(t)} y \right\|_{L^2(0,T)} &\le Q\lambda^6 \left\| e^{-K\lambda^2 t} \right\|_{L^1} \left\| {}_0I_t^{1-\alpha(t)} y \right\|_{L^2} \\ &\le Q\lambda^4 \|t^{-\alpha^*}\|_{L^1(0,T)} \|y\|_{L^2(0,T)} \\ &\le Q\lambda^4 \|y\|_{L^2(0,T)}.\end{aligned} \tag{3.22}$$

We insert the estimates (3.21)–(3.22) into (3.16) to bound $\left\| t^{\frac{\alpha(0)}{2}} y'' \right\|_{L^2(0,T)}$ by

$$\left\| t^{\frac{\alpha(0)}{2}} y'' \right\|_{L^2(0,T)} \le Q(\lambda^2 \|g\|_{L^2(0,T)} + \|g\|_{H^1(0,T)} + \lambda^3 \left|\hat{y}_0\right|), \tag{3.23}$$

thus we complete the proof of the theorem.

3.2. Regularity analysis

We prove the wellposedness and regularity estimates of models (2.6)–(2.7) and (2.8)–(2.9) based on the previous theorems.

Theorem 3.3. *Suppose $0 \le \alpha(t) < \alpha^* < 1$ for some upper bound α^*, $q \in L^2(0,T;L^2)$ and $\check{w}_0 \in \check{H}^2$, then the reduced-order problem (2.8)–(2.9) admits a unique solution $u \in L^2(0,T;\check{H}^4) \cap H^1(0,T;L^2)$ and*

$$\|u\|_{L^2(0,T;\check{H}^4)} + \|u\|_{H^1(0,T;L^2)} \le Q\big(\|q\|_{L^2(0,T;L^2)} + \|\check{w}_0\|_{\check{H}^2}\big). \tag{3.24}$$

Here $Q = Q(\rho, A, K, K_\alpha, \alpha^*, T)$. Furthermore, if $w_0 \in \check{H}^4$, the original problem (2.6)–(2.7) admits a unique solution $w \in H^1(0,T;\check{H}^4) \cap H^2(0,T;L^2)$ and

$$\|w\|_{H^1(0,T;\check{H}^4)} + \|w\|_{H^2(0,T;L^2)} \le Q\big(\|q\|_{L^2(0,T;L^2)} + \|\check{w}_0\|_{\check{H}^2} + \|w_0\|_{\check{H}^4}\big). \tag{3.25}$$

Proof. We express u and q in (2.8)–(2.9) in terms of $\{\phi_i\}_{i=1}^\infty$ [35,37,49–51]

$$\begin{aligned} u(x,t) &= \sum_{i=1}^\infty u_i(t)\phi_i(x), \quad u_i(t) := (u(\cdot,t),\phi_i), \quad t \in [0,T], \\ q(x,t) &= \sum_{i=1}^\infty q_i(t)\phi_i(x), \quad q_i(t) := (q(\cdot,t),\phi_i), \quad t \in [0,T], \end{aligned} \tag{3.26}$$

and plug the expansions into (2.8)–(2.9) to obtain that for $\forall (x,t) \in (0,l) \times (0,T]$

$$\sum_{i=1}^\infty \big[u_i'(t) + K\lambda_i^2 u_i(t) + K_\alpha \lambda_i^2 {}_0I_t^{1-\alpha(t)} u_i(t)\big]\phi_i(x) = \sum_{i=1}^\infty q_i(t)\phi_i(x)/(\rho A), \tag{3.27}$$

then u_i is the solution to the problem (2.8)–(2.9) if and only if $\{u_i\}_{i=1}^\infty$ solve

$$\begin{aligned} u_i'(t) + K\lambda_i^2 u_i(t) + K_\alpha \lambda_i^2 {}_0I_t^{1-\alpha(t)} u_i(t) &= q_i/(\rho A), \\ u_i(0) = \check{w}_{0,i} &:= (\check{w}_0, \phi_i), \quad i \ge 1. \end{aligned} \tag{3.28}$$

We apply Theorem 3.1 with $y = u_i$, $\hat{y}_0 = \check{w}_{0,i}$, $g = q_i/(\rho A)$ and $\lambda = \lambda_i$ to conclude that the problem (3.28) has a unique solution $u_i \in H^1(0,T)$ and the estimate (3.2) holds.

We then combine the estimate (3.2) to bound $\bar{u} := \int_0^t \big[\sum_{i=1}^{\infty} u_i'(s)\phi_i(x)\big]ds + \check{w}_0$ by

$$\begin{aligned}\|\partial_t \bar{u}\|^2_{L^2(0,T;L^2)} &\le \sum_{i=1}^{\infty} \|u_i'\|^2_{L^2(0,T)} \le Q \sum_{i=1}^{\infty}\big(\|q_i\|^2_{L^2(0,T)} + \lambda_i^2 \left|\check{w}_{0,i}\right|^2\big)\\ &= Q\big(\|q\|^2_{L^2(0,T;L^2)} + \|\check{w}_0\|^2_{\check{H}^2}\big).\end{aligned} \tag{3.29}$$

We note that $u_i(t) := \int_0^t u_i'(s)ds + \check{w}_{0,i}$ solves the ordinary differential equation (3.28) for $i \ge 1$. Thus, $\bar{u}$ is the solution to the problem (2.8)–(2.9). For some fixed $\gamma \ge 0$, we then combine (2.8)–(2.9) with the estimates (3.6) and (3.29) to bound

$$\begin{aligned}\|e^{-\gamma t}\bar{u}\|_{L^2(0,T;\check{H}^4)} &= \big\|e^{-\gamma t}\big(q/(\rho A) - \partial_t \bar{u} - {}_0I_t^{1-\alpha(t)}\partial_x^4 \bar{u}\big)\big\|_{L^2(0,T;L^2)}\\ &\le Q\big(\|q\|^2_{L^2(0,T;L^2)} + \|\check{w}_0\|^2_{\check{H}^2}\big) + Q\big\|(e^{-\gamma t}t^{-\alpha^*}) * (e^{-\gamma t}\|\partial_x^4\bar{u}(\cdot,t)\|_{L^2})\big\|_{L^2(0,T)}\\ &\le Q\big(\|q\|^2_{L^2(0,T;L^2)} + \|\check{w}_0\|^2_{\check{H}^2}\big) + Q\gamma^{\alpha^*-1}\|e^{-\gamma t}\bar{u}\|_{L^2(0,T;\check{H}^4)},\end{aligned} \tag{3.30}$$

choosing sufficiently large γ in (3.30) yields

$$\|\bar{u}\|_{L^2(0,T;\check{H}^4)} \le Q\big(\|q\|^2_{L^2(0,T;L^2)} + \|\check{w}_0\|^2_{\check{H}^2}\big),$$

which, together with the estimate (3.29), completes the proof of the first estimate of the theorem. The uniqueness of the solution to the model (2.8)–(2.9) follows from that for the corresponding ordinary differential equation (3.28). We further conclude that the problem (2.6)–(2.7) has a unique solution $w \in H^1(0,T;\check{H}^4) \cap H^2(0,T;L^2)$ with the stability estimate (3.25) obtained from (3.24), which completes the proof of the theorem.

We analyze high-order spatial and temporal regularity of the solutions to be used in the derivation and analysis of numerical schemes in Section 4.

Theorem 3.4. *Suppose $0 \le \alpha(t) < \alpha^* < 1$ for some upper bound α^*, $\alpha \in C^1[0,T]$, $q \in L^2(0,T;\check{H}^4) \cap H^1(0,T;L^2)$ and $\check{w}_0 \in \check{H}^6$, the following stability estimate holds for the solution u to the reduced-order problem (2.8)–(2.9)*

$$\begin{aligned}&\|u\|_{H^1(0,T;\check{H}^4)} + \big\|t^{\frac{\alpha(0)}{2}}\partial_t^2 u\big\|_{L^2(0,T;L^2)}\\ &\qquad \le Q\big(\|q\|_{L^2(0,T;\check{H}^4)} + \|q\|_{H^1(0,T;L^2)} + \|\check{w}_0\|_{\check{H}^6}\big).\end{aligned} \tag{3.31}$$

Here $Q = Q(\rho, A, K, K_\alpha, \alpha^*, \|\alpha\|_{C^1[0,T]}, T)$. If $w_0 \in \check{H}^4$, the solution w to the original problem (2.6)–(2.7) has the stability estimate

$$\begin{aligned}&\|w\|_{H^2(0,T;\check{H}^4)} + \|t^{\frac{\alpha(0)}{2}}\partial_t^3 w\|_{L^2(0,T;L^2)}\\ &\le Q\big(\|q\|_{L^2(0,T;\check{H}^4)} + \|q\|_{H^1(0,T;L^2)} + \|\check{w}_0\|_{\check{H}^6} + \|w_0\|_{\check{H}^4}\big).\end{aligned} \tag{3.32}$$

Proof. The following estimates could be performed similarly as (3.29) via the estimates in (3.2) and (3.15)

$$\begin{aligned}\|\partial_t u\|^2_{L^2(0,T;\check{H}^4)} &\le \sum_{i=1}^{\infty}\lambda_i^4\|u_i'\|^2_{L^2(0,T)} \le Q\sum_{i=1}^{\infty}\big(\lambda_i^4\|q_i\|^2_{L^2(0,T)} + \lambda_i^6\left|\check{w}_{0,i}\right|^2\big)\\ &= Q\big(\|q\|^2_{L^2(0,T;\check{H}^4)} + \|\check{w}_0\|^2_{\check{H}^6}\big),\end{aligned} \tag{3.33}$$

and

$$\begin{aligned}\big\|t^{\frac{\alpha(0)}{2}}\partial_t^2 u\big\|^2_{L^2(0,T;L^2)} &\le \sum_{i=1}^{\infty}\big\|t^{\frac{\alpha(0)}{2}}u_i''(t)\big\|^2_{L^2(0,T)}\\ &\le Q\sum_{i=1}^{\infty}\big(\lambda_i^4\|q_i\|^2_{L^2(0,T)} + \|q_i\|^2_{H^1(0,T)} + \lambda_i^6\left|\check{w}_{0,i}\right|^2\big)\\ &\le Q\big(\|q\|^2_{L^2(0,T;\check{H}^4)} + \|q\|^2_{H^1(0,T;L^2)} + \|\check{w}_0\|^2_{\check{H}^6}\big),\end{aligned} \tag{3.34}$$

we then combine the estimates (3.33)–(3.34) with the estimates (3.24)–(3.25) to complete the proof of the theorem.

4. Discretization and error estimate

4.1. Reference equation and numerical discretization

To develop and study the finite element scheme to the original problem (2.6)–(2.7), we consider the following reduced-order system [40]

$$\begin{aligned}&\partial_t u + K\partial_x^4 u + K_\alpha\, {}_0I_t^{1-\alpha(t)}\partial_x^4 u = F := q/(\rho A), \quad (x,t)\in(0,l)\times(0,T],\\ &u = \partial_t w, \qquad u(x,0) = \check{w}_0,\end{aligned}\tag{4.1}$$

Let $t_n := n\tau$ for $n = 0,1,\ldots,N$ with $\tau := T/N$ be a uniform partition on $[0,T]$, $u_n := u(x,t_n)$, $\alpha_n := \alpha(t_n)$, $F_n := F(t_n)$. Then for $1 \le n \le N$,

$$\begin{aligned}&\partial_t u(x,t_n) = \delta_\tau u_n + E_n := \frac{u_n - u_{n-1}}{\tau} + \frac{1}{\tau}\int_{t_{n-1}}^{t_n} \partial_t^2 u(x,t)(t-t_{n-1})dt,\\ &\partial_t w(x,t_n) = \delta_\tau w_n + \hat{E}_n := \frac{w_n - w_{n-1}}{\tau} + \frac{1}{\tau}\int_{t_{n-1}}^{t_n} \partial_t^2 w(x,t)(t-t_{n-1})dt,\\ &{}_0I_t^{1-\alpha(t)}\partial_x^4 u(x,t_n) = \sum_{k=1}^n \int_{t_{k-1}}^{t_k} \frac{\partial_x^4 u(x,s)ds}{\Gamma(1-\alpha(s))(t_n-s)^{\alpha(s)}}\\ &= \sum_{k=1}^n \Bigg[\int_{t_{k-1}}^{t_k} \frac{\partial_x^4 u_k ds}{\Gamma(1-\alpha_k)(t_n-s)^{\alpha_k}}\\ &\quad + \int_{t_{k-1}}^{t_k} \frac{\partial_x^4 u(x,s)ds}{\Gamma(1-\alpha(s))(t_n-s)^{\alpha(s)}} - \int_{t_{k-1}}^{t_k} \frac{\partial_x^4 u(x,s)ds}{\Gamma(1-\alpha_k)(t_n-s)^{\alpha_k}}\\ &\quad + \int_{t_{k-1}}^{t_k} \frac{\partial_x^4 u(x,s) - \partial_x^4 u_k ds}{\Gamma(1-\alpha_k)(t_n-s)^{\alpha_k}} \Bigg]\\ &:= I_\tau^{1-\alpha_n}\partial_x^4 u_n + J_n + R_n,\end{aligned}\tag{4.2}$$

where $I_\tau^{1-\alpha_n}\partial_x^4 u_n$ and the local truncation errors are given below

$$\begin{aligned}&I_\tau^{1-\alpha_n}\partial_x^4 u_n := \sum_{k=1}^n b_{n,k}\partial_x^4 u_k, \quad b_{n,k} := \int_{t_{k-1}}^{t_k} \frac{ds}{\Gamma(1-\alpha_k)(t_n-s)^{\alpha_k}},\\ &J_n = \sum_{k=1}^n \int_{t_{k-1}}^{t_k} \left[\frac{\partial_x^4 u(x,s)}{\Gamma(1-\alpha(s))(t_n-s)^{\alpha(s)}} - \frac{\partial_x^4 u(x,s)}{\Gamma(1-\alpha_k)(t_n-s)^{\alpha_k}} \right] ds,\\ &R_n = \sum_{k=1}^n \int_{t_{k-1}}^{t_k} \frac{\partial_x^4 u(x,s) - \partial_x^4 u_k ds}{\Gamma(1-\alpha_k)(t_n-s)^{\alpha_k}} = \sum_{k=1}^n \int_{t_{k-1}}^{t_k} \frac{\int_{t_k}^s \partial_\theta \partial_x^4 u(x,\theta)d\theta ds}{\Gamma(1-\alpha_k)(t_n-s)^{\alpha_k}}.\end{aligned}\tag{4.3}$$

Define $a(z,\chi) := (\partial_x^2 z, \partial_x^2 \chi)_{L^2(0,l)}$ for $z, \chi \in \check{H}^2$. We integrate the terms $\partial_x^4 u_n$ and $I_\tau^{1-\alpha_n}\partial_x^4 u_n$ for $n = 1,2,\ldots,N$ multiplied by any $\chi \in \check{H}^2$ on $(0,l)$ by parts twice in which the last two boundary conditions in (2.9) and the relations in (4.3) are employed to obtain

$$\begin{aligned}&(\partial_x^4 u_n, \chi) = \partial_x^3 u_n(x)\chi(x)\big|_{x=0}^l - (\partial_x^3 u_n, \partial_x\chi) = -(\partial_x^3 u_n, \partial_x\chi)\\ &\qquad = -\partial_x^2 u_n(x)\partial_x\chi(x)\big|_{x=0}^l + (\partial_x^2 u_n, \partial_x^2\chi) = (\partial_x^2 u_n, \partial_x^2\chi) = a(u_n,\chi),\\ &\big({}_0I_\tau^{1-\alpha_n}\partial_x^4 u_n, \chi\big) = \big(\partial_x^4[{}_0I_\tau^{1-\alpha_n}u_n], \chi\big) = -(\partial_x^3[{}_0I_\tau^{1-\alpha_n}u_n], \partial_x\chi)\\ &\qquad = -\partial_x^2[{}_0I_\tau^{1-\alpha_n}u_n]\partial_x\chi(x)\big|_{x=0}^l + (\partial_x^2[{}_0I_\tau^{1-\alpha_n}u_n], \partial_x^2\chi)\end{aligned}\tag{4.4}$$

$$= -{}_0I_\tau^{1-\alpha_n}\partial_x^2 u_n(x)\partial_x\chi(x)\Big|_{x=0}^{l} + (\partial_x^2[{}_0I_\tau^{1-\alpha_n}u_n], \partial_x^2\chi)$$
$$= (\partial_x^2[{}_0I_\tau^{1-\alpha_n}u_n], \partial_x^2\chi) = a(I_\tau^{1-\alpha_n}u_n, \chi).$$

We plug the discretizations (4.2)–(4.3) into (4.1), and integrate the resulting equation multiplied by any $\chi \in \check{H}^2$ on $(0, l)$ by parts twice to get the following equation for any $\chi \in \check{H}^2$ and $n = 1, 2, \ldots, N$ by (4.4):

$$\begin{aligned} &\big(\delta_\tau u_n, \chi\big) + Ka(u_n, \chi) + K_\alpha a(I_\tau^{1-\alpha_n}u_n, \chi) \\ &\qquad\qquad = \big(F_n, \chi\big) - (E_n + K_\alpha(J_n + R_n), \chi), \\ &u_n = \delta_\tau w_n + \hat{E}_n. \end{aligned} \tag{4.5}$$

Let $S_h \subset \check{H}^2$ be the continuously differentiable piecewise cubic Hermite finite element space on a quasi-uniform partition on $[0, l]$ with the partition diameter h. It is well known that the Ritz projection $\Pi_h : \check{H}^2 \to S_h$ [42]

$$a(\Pi_h g, \chi) = a(g, \chi), \quad \forall g \in S_h \tag{4.6}$$

has the approximation property [42]

$$\|\Pi_h g - g\|_{\check{H}^m} \le Qh^{4-m}\|g\|_{\check{H}^4}, \quad \forall g \in \check{H}^4,\ m = 0, 1, 2. \tag{4.7}$$

We drop the local truncation errors and then obtain a finite element scheme for (4.1): Find $U_n, W_n \in S_h$ for $n = 1, 2, \ldots, N$ with $U_0 := \Pi_h\check{w}_0$ and $W_0 := w_0$ such that for any $\chi \in S_h$

$$\begin{aligned} &\big(\delta_\tau U_n, \chi\big) + Ka\big(U_n, \chi\big) + K_\alpha a(I_\tau^{1-\alpha_n}U_n, \chi) = \big(F_n, \chi\big), \\ &U_n = \delta_\tau W_n, \end{aligned} \tag{4.8}$$

4.2. Estimates of local truncation error

We bound the temporal truncation error E_n, $\hat{E}_n$, J_n, R_n, and spatial truncation error with respect to $\eta(x,t) := u(x,t) - \Pi_h u(x,t)$ and $\hat{\eta}(x,t) := w(x,t) - \Pi_h w(x,t)$.

Theorem 4.1. *Suppose $0 \le \alpha(t) < \alpha^* < 1$ for some upper bound α^*, $\alpha \in C^1[0,T]$, $q \in L^2(0,T;\check{H}^4) \cap H^1(0,T;L^2)$, $\check{w}_0 \in \check{H}^6$ and $w_0 \in \check{H}^4$, then the following estimates hold*

$$\begin{aligned} &\|E\|_{\hat{L}^1(L^2)} + \|\hat{E}\|_{\hat{L}^1(L^2)} + \|R\|_{\hat{L}^1(L^2)} \le QM\tau, \quad \|E\|_{\hat{L}^1(L^2)} := \tau\sum_{n=1}^N \|E_n\|, \\ &\|\eta\|_{\hat{L}^\infty(L^2)} + \|\hat{\eta}\|_{\hat{L}^\infty(L^2)} + \|J\|_{\hat{L}^\infty(L^2)} \le QM(\tau + h^4), \\ &\|\delta_\tau\eta\|_{\hat{L}^1(L^2)} + \|\delta_\tau\hat{\eta}\|_{\hat{L}^1(L^2)} \le QMh^4, \quad \|J\|_{\hat{L}^\infty(L^2)} := \max_{1\le n\le N}\|J_n\|, \end{aligned} \tag{4.9}$$

where $M := \|q\|_{L^2(0,T;\check{H}^4)} + \|q\|_{H^1(0,T;L^2)} + \|\check{w}_0\|_{\check{H}^6} + \|w_0\|_{\check{H}^4}$ and the constant Q is independent of h, τ, N.

Proof. We use Theorems 3.3 and 3.4, Cauchy's inequality and the fact that $0 \le \alpha(0) \le \alpha^* < 1$ to bound E_n and $\hat{E}_n$ in (4.2) by

$$\begin{aligned} \|E\|_{\hat{L}^1(L^2)} &\le \tau\sum_{n=1}^N \int_{t_{n-1}}^{t_n} \big\|\partial_t^2 u(\cdot,t)\big\|_{L^2}dt = \tau\int_0^T \big\|\partial_t^2 u(\cdot,t)\big\|_{L^2}dt \\ &= \tau\int_0^T t^{-\frac{\alpha(0)}{2}}\big\|t^{\frac{\alpha(0)}{2}}\partial_t^2 u(\cdot,t)\big\|_{L^2}dt \\ &\le \tau\left(\int_0^T t^{-\alpha(0)}dt\right)^{\frac12} \times \left(\int_0^T \big\|t^{\frac{\alpha(0)}{2}}\partial_t^2 u(\cdot,t)\big\|_{L^2}^2 dt\right)^{\frac12} \\ &\le Q\tau\big\|t^{\frac{\alpha(0)}{2}}\partial_t^2 u\big\|_{L^2(0,T;L^2)} \le QM\tau, \\ \|\hat{E}\|_{\hat{L}^1(L^2)} &\le \tau\sum_{n=1}^N \int_{t_{n-1}}^{t_n} \big\|\partial_t^2 w(\cdot,t)\big\|_{L^2}dt = \tau\int_0^T \big\|\partial_t^2 w(\cdot,t)\big\|_{L^2}dt \le QM\tau, \end{aligned} \tag{4.10}$$

We combine Theorem 3.4 with the estimate $\|u\|_{C([0,T];\check{H}^4)} \le Q\|u\|_{H^1(0,T;\check{H}^4)}$, the estimate

$$\frac{|\ln(t-s)|}{(t_n-s)^{\alpha(z)}} \le Q\frac{|\ln(t-s)|}{(t_n-s)^{\alpha^*}} = Q\frac{|\ln(t-s)|\,(t-s)^{(1-\alpha*)/2}}{(t_n-s)^{(1+\alpha*)/2}} \le \frac{Q}{(t_n-s)^{(1+\alpha*)/2}}, \tag{4.11}$$

(3.6) as well as mean value theorem to obtain

$$\begin{aligned}\|J\|_{\hat{L}^\infty(L^2)} &\le Q\|u\|_{C([0,T];\check{H}^4)} \max_{1\le n\le N}\sum_{k=1}^n\int_{t_{k-1}}^{t_k}\left|\frac{(t_n-s)^{-\alpha(s)}}{\Gamma(1-\alpha(s))}-\frac{(t_n-s)^{-\alpha_k}}{\Gamma(1-\alpha_k)}\right|ds\\
&\le Q\tau\|u\|_{H^1(0,T;\check{H}^4)}\max_{1\le n\le N}\sum_{k=1}^n\int_{t_{k-1}}^{t_k}\left|\frac{\Gamma'(1-\alpha(z))\alpha'(z)}{(t_n-s)^{\alpha(z)}\Gamma^2(1-\alpha(z))}\right.\\
&\qquad\left.-\frac{\ln(t_n-s)\alpha'(z)}{\Gamma(1-\alpha(z))(t_n-s)^{\alpha(z)}}\right|ds\\
&\le Q\tau\|u\|_{H^1(0,T;\check{H}^4)}\max_{1\le n\le N}\sum_{k=1}^n\int_{t_{k-1}}^{t_k}\frac{1}{(t_n-s)^{(1+\alpha*)/2}}ds \le QM\tau,\end{aligned} \tag{4.12}$$

We utilize the estimates in Theorem 3.4 and consider the estimate of R_n for $1\le n\le N$

$$\begin{aligned}&\|R\|_{\hat{L}^1(L^2)} \le Q\tau\sum_{n=1}^N\sum_{k=1}^n\int_{t_{k-1}}^{t_k}\frac{\int_{t_k}^s\|\partial_\theta u(\cdot,\theta)\|_{\check{H}^4}}{(t_n-s)^{\alpha_k}}d\theta ds\\
&\le Q\tau\sum_{k=1}^n\int_{t_{k-1}}^{t_k}\|\partial_\theta u(\cdot,\theta)\|_{\check{H}^4}\sum_{n=k}^N\int_{t_{k-1}}^{t_k}(t_n-s)^{-\alpha_k}dsd\theta\\
&\le Q\tau\sum_{k=1}^n(T-t_{k-1})^{1-\alpha^*}\int_{t_{k-1}}^{t_k}\|\partial_\theta u(\cdot,\theta)\|_{\check{H}^4}d\theta \le Q\tau\|u\|_{W^{1,1}(0,T;\check{H}^4)} \le QM\tau.\end{aligned} \tag{4.13}$$

We finally use (4.7) and Theorem 3.4 to bound $\eta_n := u_n - \Pi_h u_n$ by

$$\begin{aligned}&\|\eta\|_{\hat{L}^\infty(L^2)} \le Qh^4\|u\|_{C([0,T];\check{H}^4)} \le QMh^4,\\
&\|\delta_\tau\eta\|_{\hat{L}^1(L^2)} = \sum_{n=1}^N\left\|\int_{t_{n-1}}^{t_n}(I-\Pi_h)\partial_t u dt\right\| \le Qh^4\|u\|_{W^{1,1}(0,T;\check{H}^4)} \le QMh^4,\end{aligned} \tag{4.14}$$

and we can similarly bound $\hat{\eta}$ and $\delta_\tau\hat{\eta}$ and thus finish the proof of (4.9).

4.3. Error estimate for the finite element scheme

Theorem 4.2. *Suppose $0 \le \alpha(t) < \alpha^* < 1$ for some upper bound α^*, $\alpha \in C^1[0,T]$, $q \in L^2(0,T;\check{H}^4) \cap H^1(0,T;L^2)$, $\check{w}_0 \in \check{H}^6$ and $w_0 \in \check{H}^4$, the optimal-order error estimate holds for the finite element scheme (4.8) defined on the uniform temporal mesh*

$$\|w-W\|_{\hat{L}^\infty(L^2)} + \|\partial_t w - U\|_{\hat{L}^\infty(L^2)} \le QM(\tau+h^4), \tag{4.15}$$

where $Q = Q(\rho, A, K, K_\alpha, \alpha^*, \|\alpha\|_{C^1[0,T]}, T)$ and $M = \|q\|_{L^2(0,T;\check{H}^4)} + \|q\|_{H^1(0,T;L^2)} + \|\check{w}_0\|_{\check{H}^6} + \|w_0\|_{\check{H}^4}$.

Proof. We decompose the global truncation error $u_n - U_n = \xi_n + \eta_n$ with $\xi_n := \Pi_h u_n - U_n \in S_h$ and $w_n - W_n = \hat{\xi}_n + \hat{\eta}_n$ with $\hat{\xi}_n := \Pi_h w_n - W_n \in S_h$. We subtract (4.8) from (4.5) and employ (4.6) to obtain that for $\chi \in S_h$ and $1 \le n \le N$,

$$\begin{aligned}&\big(\delta_\tau\xi_n,\chi\big) + Ka\big(\xi_n,\chi\big) + K_\alpha a\big(I_\tau^{1-\alpha_n}\xi_n,\chi\big) = -(G_n,\chi),\\
&\hat{\xi}_n = \hat{\xi}_{n-1} + \tau\big(\xi_n + \eta_n - \hat{E}_n - \delta_\tau\hat{\eta}_n\big),\end{aligned} \tag{4.16}$$

where $G_n = K_\alpha(J_n + R_n) + \delta_\tau \eta_n + E_n$ for $1 \le n \le N$. For a fixed $\mu > 0$, let $\breve{\xi}_n = e^{-\mu t_n}\xi_n$ for $1 \le n \le N$. We incorporate the following relations

$$\begin{aligned}
&e^{-\mu t_n}\delta_\tau \xi_n = \tau^{-1}\big[e^{-\mu t_n}\xi_n - e^{-\mu t_{n-1}}\xi_{n-1} + e^{-\mu t_{n-1}}\xi_{n-1} - e^{-\mu t_n}\xi_{n-1}\big]\\
&\qquad\qquad\quad = \delta_\tau \breve{\xi}_n + \tau^{-1}(1 - e^{-\mu\tau})\breve{\xi}_{n-1},\\
&e^{-\mu t_n} a\big(I_\tau^{1-\alpha_n}\xi_n, \chi\big) = e^{-\mu t_n}\sum_{k=1}^n b_{n,k} a(\xi_k, \chi)\\
&\qquad = \sum_{k=1}^n \int_{t_{k-1}}^{t_k} \frac{e^{-\mu(t_n - t_k)} e^{-\mu t_k} a(\xi_k, \chi) ds}{\Gamma(1-\alpha_k)(t_n - s)^{\alpha_k}} = \sum_{k=1}^n \breve{b}_{n,k} a(\breve{\xi}_k, \chi),\\
&\breve{b}_{n,k} = \int_{t_{k-1}}^{t_k} \frac{e^{-\mu(t_n - t_k)} ds}{\Gamma(1-\alpha_k)(t_n - s)^{\alpha_k}}, \quad 1 \le k \le n \le N
\end{aligned} \tag{4.17}$$

with the first equation multiplied by $e^{-\mu t_n}$ in (4.16) and $\chi = \breve{\xi}_n$ to obtain

$$\begin{aligned}
&\big(\delta_\tau \breve{\xi}_n, \breve{\xi}_n\big) + \frac{(1 - e^{-\mu\tau})}{\tau}(\breve{\xi}_{n-1}, \breve{\xi}_n) + K a\big(\breve{\xi}_n, \breve{\xi}_n\big)\\
&\qquad\qquad + K_\alpha \sum_{k=1}^n \breve{b}_{n,k} a(\breve{\xi}_k, \breve{\xi}_n) = -e^{-\mu t_n}(G_n, \breve{\xi}_n),\\
&\hat{\xi}_n = \hat{\xi}_{n-1} + \tau\big(\xi_n + \eta_n - \hat{E}_n - \delta_\tau \hat{\eta}_n\big).
\end{aligned} \tag{4.18}$$

We employ the fact

$$\tau\big(\delta_\tau \breve{\xi}_n, \breve{\xi}_n\big) + (1 - e^{-\mu\tau})(\breve{\xi}_{n-1}, \breve{\xi}_n) = \|\xi_n\|^2 - e^{-\mu\tau}(\breve{\xi}_{n-1}, \breve{\xi}_n),$$

and multiply the first equation in (4.18) by 2τ and then use geometric–arithmetic inequality to cancel $\|\breve{\xi}_n\|^2$ on both sides to obtain

$$\|\breve{\xi}_n\|^2 + 2K\tau\|\partial_x^2 \breve{\xi}_n\|^2 \le \|\breve{\xi}_{n-1}\|^2 + K_\alpha \tau \sum_{k=1}^n \breve{b}_{n,k}\big(\|\partial_x^2 \breve{\xi}_k\|^2 + \|\partial_x^2 \breve{\xi}_n\|^2\big) + 2\tau\|G_n\|\|\breve{\xi}_n\|.$$

We then sum the above inequality from $n = 1$ to n_0 for $1 \le n_0 \le N$ and cancel the like terms on both sides to obtain

$$\begin{aligned}
\|\breve{\xi}_{n_0}\|^2 + 2K\tau \sum_{n=1}^{n_0} \|\partial_x^2 \breve{\xi}_n\|^2 \le K_\alpha \tau \sum_{n=1}^{n_0}\sum_{k=1}^n \breve{b}_{n,k}(\|\partial_x^2 \breve{\xi}_k\|^2 + \|\partial_x^2 \breve{\xi}_n\|^2)\\
+ 2\tau \sum_{n=1}^{n_0} \|G_n\|\|\breve{\xi}_n\|.
\end{aligned} \tag{4.19}$$

To estimate the first two terms on the right hand side of (4.19), we define the sequences $\boldsymbol{\zeta} = \{\zeta_n\}_{n=1}^N = \big\{\|\partial_x^2 \breve{\xi}_n\|^2\big\}_{n=1}^N$, $\boldsymbol{B} = \{B_n\}_{n=1}^N$ with $B_n = \int_{-\tau}^0 \frac{e^{-\mu(t_n - s)}ds}{(t_n - s)^{\alpha^*}}$ for $1 \le n \le N$ and

$$\begin{aligned}
&\|\boldsymbol{\zeta}\|_{l_1} := \sum_{n=1}^N \|\partial_x^2 \breve{\xi}_n\|^2,\\
&\|\boldsymbol{B}\|_{l_1} = \sum_{n=1}^N |B_n| = \sum_{n=1}^N \int_{-\tau}^0 \frac{e^{-\mu(t_n - s)}ds}{(t_n - s)^{\alpha^*}} = \sum_{n=1}^N \int_{t_n}^{t_{n+1}} e^{-\mu s} s^{-\alpha^*} ds\\
&\qquad\quad \le \int_0^\infty e^{-\mu s} s^{-\alpha^*} ds \le Q\mu^{\alpha^* - 1}.
\end{aligned} \tag{4.20}$$

The estimate (4.20) together with (4.17) and discrete Young's convolution formula yields

$$
\begin{aligned}
\tau\sum_{n=1}^{n_0}\sum_{k=1}^{n}\breve{b}_{n,k}\|\partial_x^2\breve{\xi}_k\|^2 &= \tau\sum_{n=1}^{n_0}\sum_{k=1}^{n}\int_{t_{k-1}}^{t_k}\frac{e^{-\mu(t_n-t_k)}ds}{\Gamma(1-\alpha_k)(t_n-s)^{\alpha_k}}\|\partial_x^2\breve{\xi}_k\|^2\\
&\le Qe^{\mu\tau}\tau\sum_{n=1}^{n_0}\sum_{k=1}^{n}\int_{t_{k-1}}^{t_k}\frac{e^{-\mu(t_n-s)}ds}{(t_n-s)^{\alpha^*}}\zeta_k\\
&\le Qe^{\mu\tau}\tau\sum_{n=1}^{n_0}\sum_{k=1}^{n}\int_{-\tau}^{0}\frac{e^{-\mu(t_n-t_k-s)}ds}{(t_n-t_k-s)^{\alpha^*}}\zeta_k\\
&= Qe^{\mu\tau}\tau\sum_{n=1}^{n_0}\big(\boldsymbol{B}*\boldsymbol{\zeta}\big)_n \le Qe^{\mu\tau}\tau\big\|\boldsymbol{B}*\boldsymbol{\zeta}\big\|_{l_1}\\
&\le Qe^{\mu\tau}\tau\|\boldsymbol{B}\|_{l_1}\|\boldsymbol{\zeta}\|_{l_1} \le Qe^{\mu\tau}\mu^{\alpha^*-1}\tau\sum_{n=1}^{n_0}\|\partial_x^2\breve{\xi}_n\|^2,
\end{aligned}
\tag{4.21}
$$

and

$$
\begin{aligned}
&\tau\sum_{n=1}^{n_0}\sum_{k=1}^{n}\breve{b}_{n,k}\|\partial_x^2\breve{\xi}_n\|^2 = \tau\sum_{n=1}^{n_0}\|\partial_x^2\breve{\xi}_n\|^2\sum_{k=1}^{n}\breve{b}_{n,k}\\
&\quad\le e^{\mu\tau}\tau\sum_{n=1}^{n_0}\|\partial_x^2\breve{\xi}_n\|^2\sum_{k=1}^{n}\int_{t_{k-1}}^{t_k}\frac{e^{-\mu(t_n-s)}ds}{\Gamma(1-\alpha_k)(t_n-s)^{\alpha_k}}\\
&\quad\le Qe^{\mu\tau}\tau\sum_{n=1}^{n_0}\|\partial_x^2\breve{\xi}_n\|^2\int_0^{t_n}\frac{e^{-\mu(t_n-s)}ds}{(t_n-s)^{\alpha^*}} \le Qe^{\mu\tau}\mu^{\alpha^*-1}\tau\sum_{n=1}^{n_0}\|\partial_x^2\breve{\xi}_n\|^2.
\end{aligned}
\tag{4.22}
$$

Then the left hand side terms in (4.19) can be estimated by

$$
\|\breve{\xi}_{n_0}\|^2 + K\tau\sum_{n=1}^{n_0}\|\partial_x^2\breve{\xi}_n\|^2 \le Q_1K_\alpha e^{\mu\tau}\mu^{\alpha_*-1}\tau\sum_{n=1}^{n_0}\|\partial_x^2\breve{\xi}_n\|^2 + 2\tau\sum_{n=1}^{n_0}\|G_n\|\|\breve{\xi}_n\|,
\tag{4.23}
$$

we choose μ sufficiently large to ensure $Q_1K_\alpha\mu^{\alpha_*-1}e^{\mu\tau} < K$ to arrive at

$$
\|\breve{\xi}_{n_0}\|^2 \le Q\tau\sum_{n=1}^{n_0}\|G_n\|\|\breve{\xi}_n\|.
\tag{4.24}
$$

Let $\|\breve{\xi}_{n_*}\| := \max_{1\le n\le N}\|\breve{\xi}_n\|$ (assumed positive without loss of generality). Set $n_0 = n_*$ in (4.24), divide the resulting inequality by $\|\breve{\xi}_{n_*}\|$ and utilize the estimates in (4.9) as well as $\|\xi_n\| \le Q\|\breve{\xi}_n\|$ for $1\le n\le N$ to arrive at

$$
\|\xi_n\| \le QM(\tau+h^4),\quad 1\le n\le N.
\tag{4.25}
$$

To estimate $\hat{\xi}_n$, we sum the second equation in (4.16) from $n=1$ to n_0 to obtain

$$
\|\hat{\xi}_{n_0}\| \le Q\tau\sum_{n=1}^{n_0}\big(\|\xi_n\|+\|\eta_n\|+\|\hat{E}_n\|+\|\delta_\tau\hat{\eta}_n\|\big),\quad 1\le n_0\le N.
\tag{4.26}
$$

We then combine the estimates (4.9), (4.25) with (4.26) to bound

$$
\|\hat{\xi}_{n_0}\| \le Q(\tau+h^4),\quad 1\le n_0\le N,
\tag{4.27}
$$

and we finally incorporate (4.25) and (4.27) with preceding estimates (4.9) to complete the proof of the theorem.

5. Numerical experiments

We perform numerical experiments to investigate the convergence behavior of the proposed numerical scheme (4.8) to the model (2.6)–(2.7) and the dynamic response of the viscoelastic Euler–Bernoulli beam (2.6)–(2.7) in the context of real isotropic material, in comparison with the classical Euler–Bernoulli beam model [17]

$$
\rho A\partial_t^2 w + \varsigma\rho A\partial_t w + EI\partial_x^4 w = q(x,t),
\tag{5.1}
$$

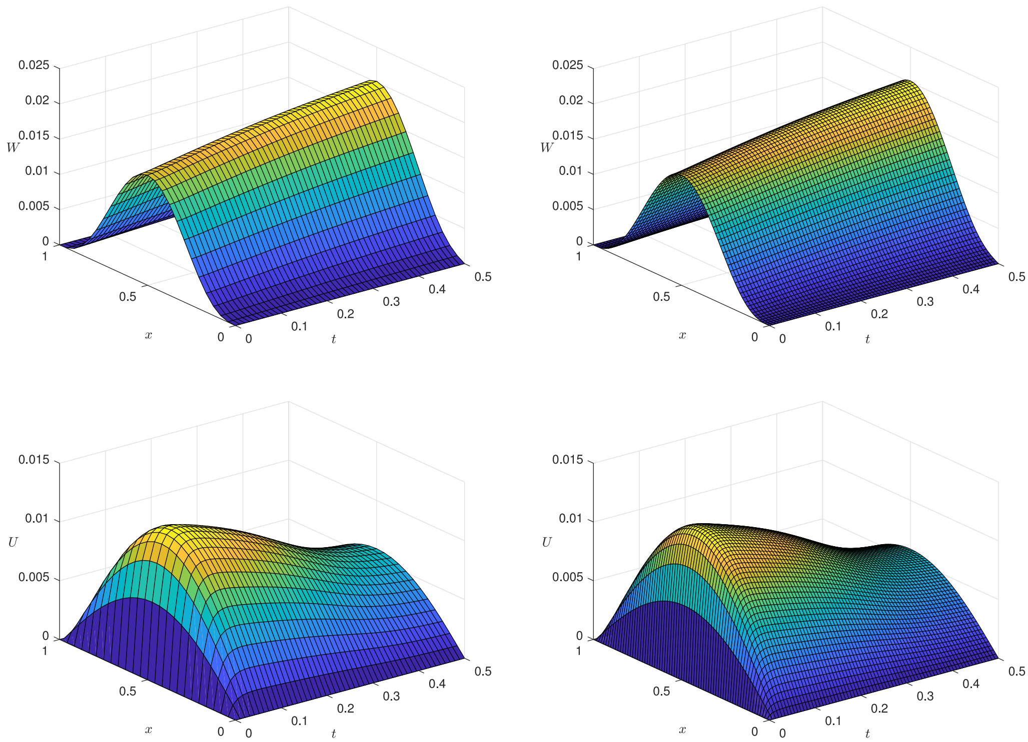

Fig. 2. Left to right: Representative plots of the numerical solutions and reference solutions in *Example* 1 with $(\alpha_0, \alpha_T) = (0, 0.6)$. First row: Space–time surface of W. Second row: Space–time surface of U.

where ς is the external damped ratio and E is the elastic modulus. The initial and boundary conditions are specified in (2.7).

5.1. Convergence of the finite element scheme

We numerically investigate the temporal and spatial convergence behavior of the finite element scheme (4.8) for the model (2.6)–(2.7) under uniform temporal and spatial partitions with the mesh size τ and h.

Example 1. Let $[0, T] = [0, 0.5]$s, $l = 1$, $E = E_d = I = \rho = A = 1$ for simplicity, $w_0(x) = x^3(1-x)^3$, $\check{w}_0 = 0$ and $q \equiv 1$ within the beam. The variable-order $\alpha(t)$ in the model (2.6)–(2.7) is defined by

$$\alpha(t) = \alpha_T + (\alpha_0 - \alpha_T)\left(1 - \frac{t}{T} - \frac{\sin(2\pi(1 - t/T))}{2\pi}\right) \tag{5.2}$$

with (i) $(\alpha_0, \alpha_T) = (0, 0.6)$, (ii) $(\alpha_0, \alpha_T) = (0.2, 0.8)$, and (iii) $(\alpha_0, \alpha_T) = (0.7, 0.3)$.

Since the analytic solution to the model (2.6)–(2.7) is not in the closed form, we accept the numerical solution computed with fine mesh size $(h_f, \tau_f) = (1/72, 1/1440)$ as a reference solution to measure the temporal convergence order and fine mesh size $(h_f, \tau_f) = (1/60, 1/8192)$ as a reference solution for the spatial convergence order. In Fig. 2, we show the representative plots of the numerical solutions and reference solutions for $(\alpha_0, \alpha_T) = (0, 0.6)$ in (5.2), computed with $(h, \tau) = (1/24, 1/48)$ and a fine mesh size $(h_f, \tau_f) = (1/72, 1/1440)$, respectively.

In the numerical experiments, we investigate the temporal convergence order ι and spatial convergence order ϑ such that,

$$\|U - \partial_t w\|_{\hat{L}^\infty(L^2)} + \|w - W\|_{\hat{L}^\infty(L^2)} \le Q(\tau^\iota + h^\vartheta). \tag{5.3}$$

When we measure ι, we adopt the same mesh size h as used for the reference solution and vice versa. We present the numerical results in Tables 1–2, and we observe first order accuracy in time and fourth order accuracy in space, which are in a good agreement with theoretical results.

Table 1
Numerical results of $\|w - W\|_{\hat{L}^\infty(L^2)}$ for the finite element scheme (4.8) of cases (i)–(iii) in Example 1.

τ	(i)	ι	(ii)	ι	(iii)	ι
1/16	$7.75E-05$	–	$6.66E-05$	–	$1.48E-05$	–
1/24	$5.20E-05$	0.98	$4.50E-05$	0.97	$9.68E-06$	1.04
1/32	$3.89E-05$	1.01	$3.39E-05$	0.99	$7.15E-06$	1.05
1/48	$2.56E-05$	1.03	$2.24E-05$	1.02	$4.63E-06$	1.07
h	(i)	ϑ	(ii)	ϑ	(iii)	ϑ
1/2	$2.32E-07$	–	$2.05E-07$	–	$2.49E-07$	–
1/3	$4.46E-08$	4.06	$3.95E-08$	4.06	$4.79E-08$	4.06
1/4	$1.40E-08$	4.04	$1.24E-08$	4.04	$1.50E-08$	4.04
1/5	$5.70E-09$	4.02	$5.04E-09$	4.02	$6.11E-09$	4.02

Table 2
Numerical results of $\|\partial_t w - U\|_{\hat{L}^\infty(L^2)}$ for the finite element scheme (4.8) of cases (i)–(iii) in Example 1.

τ	(i)	ι	(ii)	ι	(iii)	ι
1/16	$7.50E-05$	–	$7.84E-05$	–	$5.61E-06$	–
1/24	$5.04E-05$	0.98	$5.23E-05$	1.00	$3.81E-06$	0.96
1/32	$3.78E-05$	1.00	$3.89E-05$	1.03	$2.90E-06$	0.95
1/48	$2.50E-05$	1.02	$2.55E-05$	1.04	$1.97E-06$	0.95
h	(i)	ϑ	(ii)	ϑ	(iii)	ϑ
1/2	$2.87E-07$	–	$8.57E-08$	–	$3.58E-07$	–
1/3	$5.54E-08$	4.06	$1.65E-08$	4.06	$6.88E-08$	4.06
1/4	$1.74E-08$	4.03	$5.17E-09$	4.04	$2.15E-08$	4.04
1/5	$7.07E-09$	4.02	$2.11E-09$	4.02	$8.78E-09$	4.02

Table 3
Numerical results of $\|w - W\|_{\hat{L}^\infty(L^2)}$ for the finite element scheme (4.8) of cases (iv)–(vi) in Example 2.

τ	(iv)	ι	(v)	ι	(vi)	ι
1/16	$2.22E-05$	–	$6.45E-05$	–	$4.16E-06$	–
1/24	$1.46E-05$	1.03	$4.31E-05$	1.00	$2.75E-06$	1.02
1/32	$1.08E-05$	1.04	$3.22E-05$	1.01	$2.04E-06$	1.04
1/48	$7.06E-06$	1.06	$2.12E-05$	1.04	$1.32E-06$	1.06
h	(iv)	ϑ	(v)	ϑ	(vi)	ϑ
1/2	$3.28E-05$	–	$3.11E-05$	–	$2.97E-05$	–
1/3	$6.78E-06$	3.88	$6.44E-06$	3.88	$6.15E-06$	3.88
1/4	$2.18E-06$	3.95	$2.07E-06$	3.95	$1.97E-06$	3.95
1/5	$8.98E-07$	3.97	$8.52E-07$	3.97	$8.14E-07$	3.97

Example 2. Let $[0, T] = [0, 0.5]$s, $E = E_d = I = \rho = A = 1$ for simplicity, $w_0(x) = \sin(\pi x)$, $\check{w}_0 = \sin(\pi x)$ and $q \equiv 1$ within the beam. The variable-order $\alpha(t)$ in the model (2.6)–(2.7) is chosen as (iv) $\alpha(t) = 0.2 + 0.2t$, (v) $\alpha(t) = 0.5 + 0.3\sin(\pi t)$, (vi) $\alpha(t) = 0.4 + 0.1e^{-t}$. We use the numerical solution computed with fine mesh size $(h_f, \tau_f) = (1/48, 1/1440)$ as a reference solution to measure the temporal convergence order of the scheme (4.8) and fine mesh size $(h_f, \tau_f) = (1/60, 1/8192)$ as a reference solution for the spatial convergence order. In Fig. 3, we similarly show the representative plots of the numerical solutions and reference solutions for $\alpha(t) = 0.2 + 0.2t$, computed with $(h, \tau) = (1/24, 1/48)$ and a fine mesh size $(h_f, \tau_f) = (1/72, 1/1440)$, respectively. Numerical results $\|w - W\|_{\hat{L}^\infty(L^2)}$ and $\|\partial_t w - U\|_{\hat{L}^\infty(L^2)}$ are presented in Tables 3–4, which again show first order convergence in time and fourth order accuracy in space as proved in Theorem 4.2.

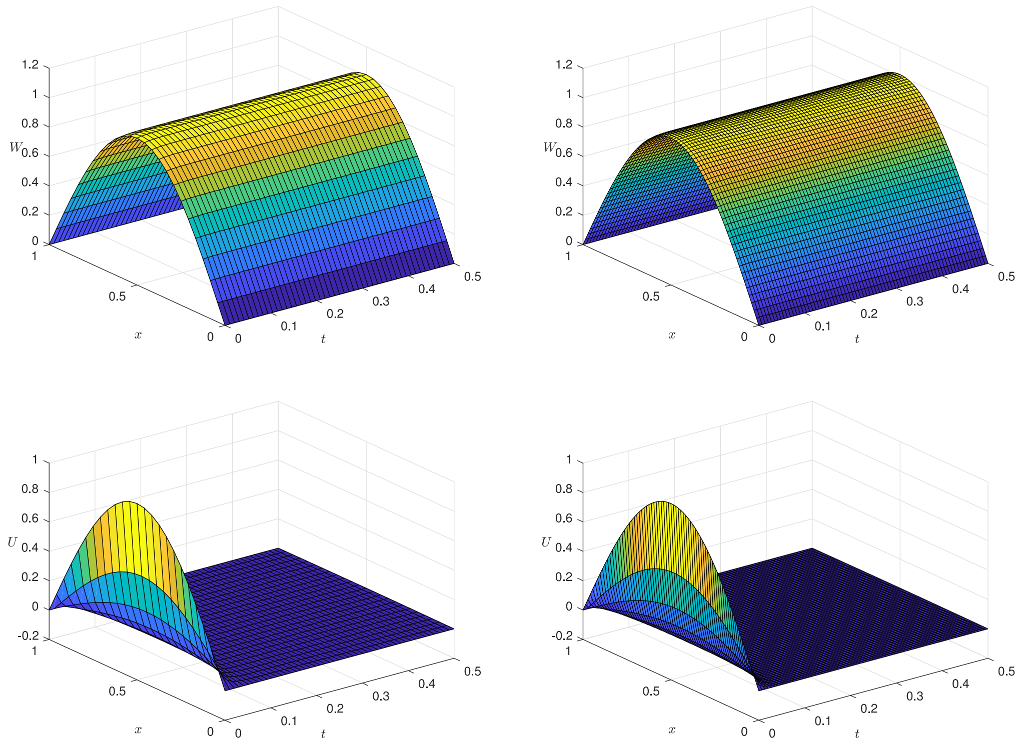

Fig. 3. Left to right: Representative plots of the numerical solutions and reference solutions in *Example* 2 with $\alpha(t) = 0.2 + 0.2t$. First row: Space–time surface of W. Second row: Space–time surface of U.

Table 4
Numerical results of $\|\partial_t w - U\|_{\hat{L}^\infty(L^2)}$ for the finite element scheme (4.8) of cases (iv)–(vi) in Example 2.

τ	(iv)	ι	(v)	ι	(vi)	ι
1/16	$1.93E-05$	–	$9.44E-05$	–	$8.26E-05$	–
1/24	$1.22E-05$	1.12	$6.23E-05$	1.02	$5.41E-05$	1.04
1/32	$8.92E-06$	1.10	$4.61E-05$	1.05	$4.00E-05$	1.05
1/48	$5.72E-06$	1.10	$3.00E-05$	1.06	$2.60E-05$	1.06
h	(iv)	ϑ	(v)	ϑ	(vi)	ϑ
1/2	$2.72E-05$	–	$1.50E-05$	–	$1.65E-05$	–
1/3	$5.63E-06$	3.88	$3.10E-06$	3.88	$3.42E-06$	3.88
1/4	$1.81E-06$	3.95	$9.96E-07$	3.95	$1.10E-06$	3.95
1/5	$7.46E-07$	3.97	$4.11E-07$	3.97	$4.53E-07$	3.97

Remark 5.1. We note that there are some existing numerical methods for the constant-order fractional Euler–Bernoulli beam (5.4), e.g., compact difference method [21], quasi-Legendre polynomial method [45], shifted Chebyshev polynomials algorithm [44], and spectral Galerkin method [41]. In particular, compared with the work [21], we specifically focus on the first-order temporal discretization scheme based on the regularity results in Theorems 3.3 and 3.4. High order discretization scheme [27,28] can definitely produce the solution with higher-order accuracy, provided that the exact solution has required high-order regularity estimates that will be investigated in the near future.

Table 5
The simulation parameters of HDPE and PEEK in model (5.4) [44].

Material	$\rho(\mathrm{kg/m^3})$	α	E_α
HDPE	960	0.1603	3.341×10^5
PEEK	1290	0.2341	5.50×10^6

5.2. Validation and comparison

The constant-order fractional Euler–Bernoulli beam

$$\rho A \partial_t^2 w + E_\alpha I \partial_t^\alpha \partial_x^4 w = q(x,t), \quad (x,t) \in (0,l) \times (0,T] \tag{5.4}$$

has been widely investigated in the literature [8,21,44,45] to describe the vibration behavior of the viscoelastic beam under external excitations. To validate the efficiency and accuracy of our developed numerical scheme (4.8), we are now in the position to compare the numerical results obtained from (4.8) by choosing $E_d = 0$ and a constant fractional order α with those existing in the literature [44,45].

In the numerical experiments, we consider two kinds of viscoelastic polymeric materials: High density polyethylene (HDPE) and Poly (ether ether ketone) (PEEK). The material parameters are listed in Table 5.

We also assume the beam to be clamped–clamped at both ends with homogeneous initial conditions in (2.7), leading to

$$\begin{aligned} w(0,t) = w(l,t) = \partial_x w(0,t) = \partial_x w(l,t) = 0, &\qquad t \in [0,T], \\ w(x,0) = \partial_t w(x,0) = 0, &\qquad x \in [0,l]. \end{aligned} \tag{5.5}$$

The beams are set to have length $l = 5$m, width 0.2 m and height 0.2 m. The moment of inertia of the beam is thus $I = \frac{0.2^4}{12} m^4$. Let $T = 2$s, the fractional Euler–Bernoulli beam model (5.4)–(5.5) is simulated via the developed finite element scheme (4.8) with the uniform spatial partition $h = 1/20$ and the uniform temporal mesh $\tau = 1/1024$. We plot the transverse deflection of the HDPE and PEEK beam under different external excitations in Fig. 4. The simulation results in Fig. 4 are quantitatively consistent with those obtained by shifted Chebyshev polynomial algorithm [44, Figure 10], which further indicates the efficiency and reliability of the proposed finite element scheme (4.8).

5.3. Model investigation

Resonance phenomenon is a critical factor determining the durability and reliability of the mechanical and biological systems, and thus it is of fundamental significance to precisely model and characterize the resonance behavior for the elongation of the durability and reliability of those systems. Since the free vibration of the beam structures with non-vanishing initial deflection or velocity will die off in the long run and we are mainly interested in mechanical and biological durability and reliability, we assume the homogeneous initial conditions and thus focus on the steady state response of the system.

We investigate the performance and behavior of the aforementioned Euler–Bernoulli beams made of Inconel alloy 718 material [16], which can work in a diverse temperature environment to provide superior tensile, creep-rupture strength, fatigue and oxidation resistance. The beams are set to have length $l = 1$m, width 0.1 m and height 0.01 m and the material data is as follows: $\rho = 8192$ kg/m^3 and $E = 200$ GPa, which give the primary frequency of the classical Euler–Bernoulli beam (5.1) as $\omega_1 = 141$ rad/s [17]. In the numerical examples, a harmonic force $q = \cos(\omega_1 t)\delta(x - l/2)$ is applied at the center of the simply-supported Euler–Bernoulli beams over the time interval $[0,T] = [0,2]$s.

The Euler–Bernoulli beam models are simulated via the proposed finite element scheme (4.8) with the uniform spatial partition $h = 1/64$. We investigate the resonance behaviors of the midpoint of neutral beam axis of the classical Euler–Bernoulli beam (5.1) without external damping in Fig. 5, from which we notice that insufficient temporal partitions cannot properly present the resonance behavior as described by the physical model and often result in nonphysical and spurious phenomena "beat", i.e., the vibration oscillates rapidly with slowly varying

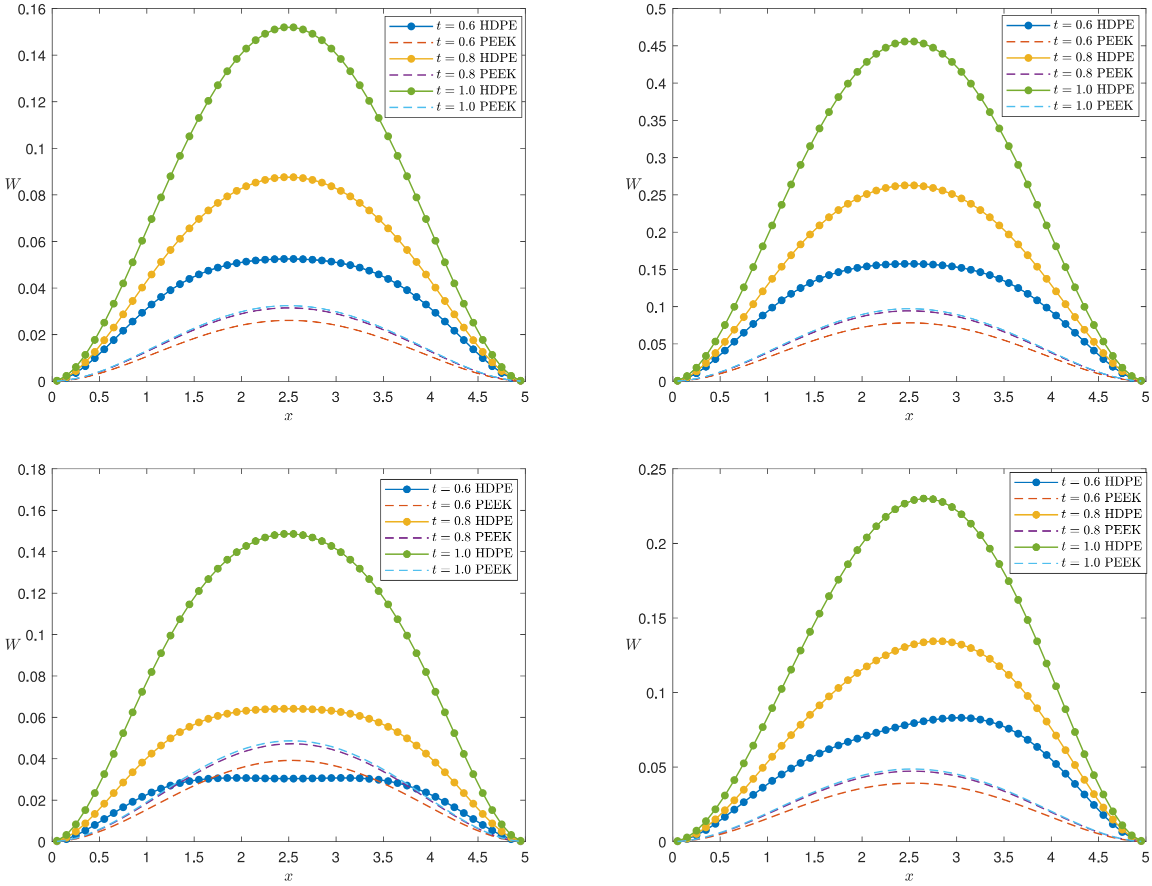

Fig. 4. Comparison of the deflection of the HDPE and PEEK beams under different external excitations. First row: $q = 10$, and $q = 30$. Second row: $q = 10\pi \sin(t)$, and $q = 10 + 2x$.

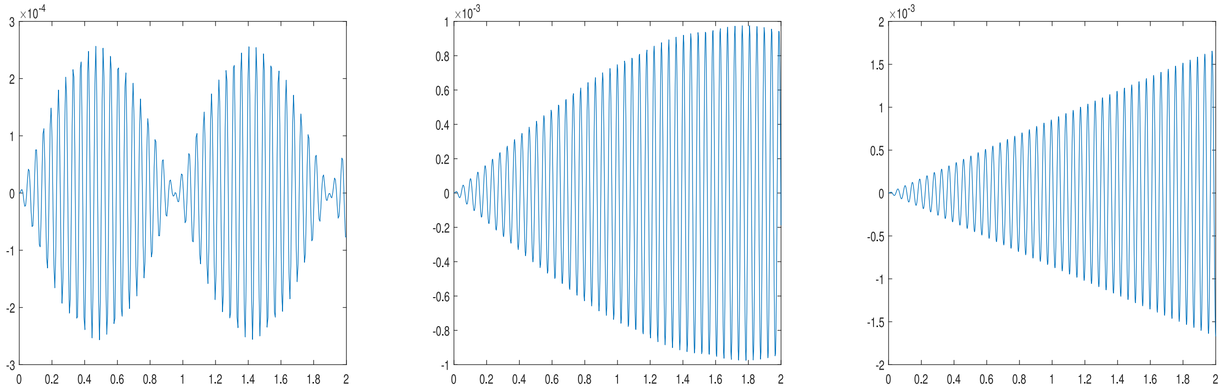

Fig. 5. Left to right: Deflection of the classical Euler–Bernoulli beam (5.1) on $[0, T]$ for $T = 2$s with $\tau = \frac{\pi}{4\omega_1}$, $\tau = \frac{\pi}{8\omega_1}$, and $\tau = \frac{\pi}{16\omega_1}$, respectively.

amplitude [17]. Hence, a fine temporal step size $\tau = \frac{\pi}{32\omega_1}$ is chosen to ensure the temporal resolution to catch physical behaviors.

We investigate the time evolution of the transverse deflection of the Euler–Bernoulli beams at the midpoint of the neural axis in Figs. 6–8. When the natural frequency of the Euler Bernoulli beam equals the driving frequency of

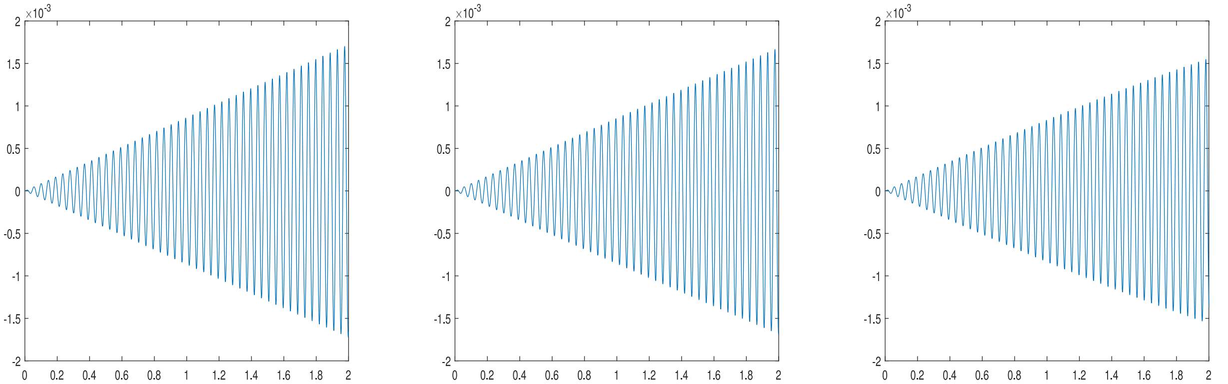

Fig. 6. Left to right: Deflection of the damped classical Euler–Bernoulli beam (5.1) on $[0, T]$ with $T = 2$s, $\varsigma = 0.01$, $\varsigma = 0.05$, and $\varsigma = 0.1$, respectively.

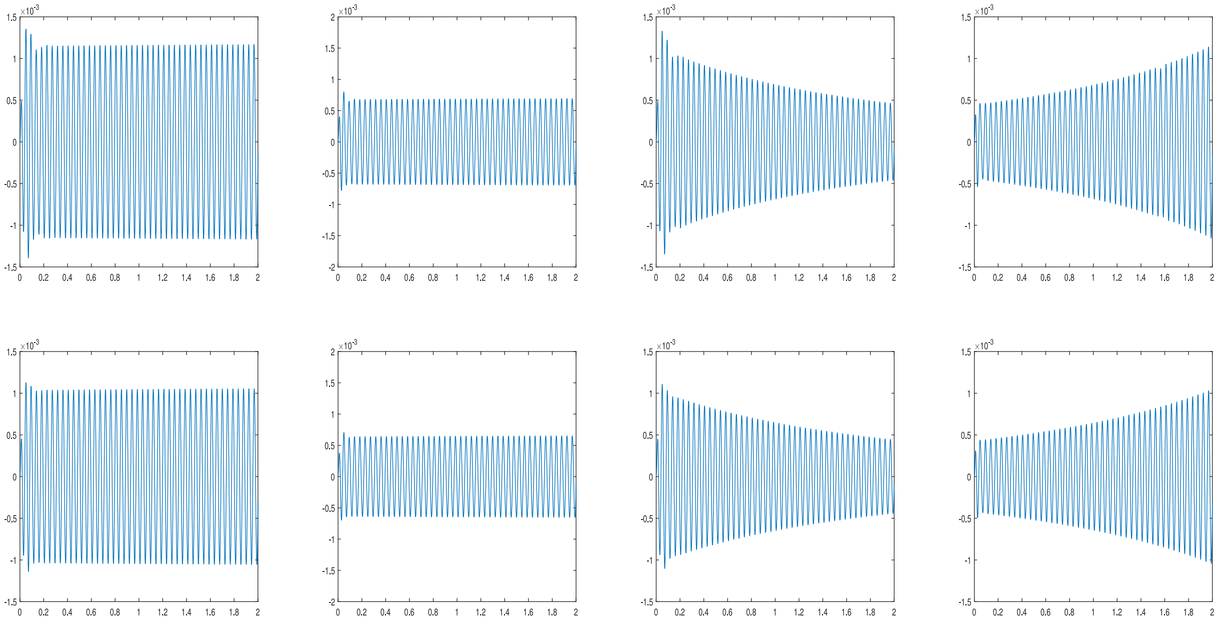

Fig. 7. Left to right: Deflection of the viscoelastic Euler–Bernoulli beam (2.6)–(2.7) on $[0, T]$ with $T = 2$s, $\alpha(t) = 0.1$, $\alpha(t) = 0.15$, $\alpha(t) = 0.1 + 0.05t$, and $\alpha(t) = 0.2 - 0.05t$, respectively. Row 1 : $E_d = 0$. Row 2: $E_d = 0.001E$.

the periodic external force applied to the beam system, (i) Fig. 6 shows that the damped classical Euler–Bernoulli beam model (5.1) predicts vibration that grows linearly in time which is in sharp contrast with the single-degree mass–spring–dashpot system [17]. In addition, we observe from Fig. 7 that viscoelastic Euler–Bernoulli beam model (2.6)–(2.7) with the inherent damping mechanism generates stable predictions of vibrations that do not grow unboundedly; (ii) we also observe from Fig. 7 that the maximal amplitude of the viscoelastic Euler–Bernoulli beam model (2.6)–(2.7) for the case $E_d = 0$ ranges from $1.2E - 3$ to $6E - 4$ with the constant α increasing from 0.1 to 0.15, and similar conclusions can be drawn for the case $E_d = 0.001E$. These observations are consistent with the discussions in Section 1; (iii) we observe from Fig. 8 that the maximal amplitude of the viscoelastic Euler–Bernoulli beam model (2.6)–(2.7) ranges from $1E - 3$ to $4E - 4$ with the internal damping coefficient E_d growing from $E_d = 0.001E$ to $E_d = 0.01E$, which decreases further to $3E - 5$ for $E_d = 0.2E$. These findings are consistent with preceding discussions in Section 2; (iv) the viscoelastic Euler–Bernoulli beam model (2.6)–(2.7), which provides more modeling compatibility and flexibility via different choices of the variable-order $\alpha(t)$, brings

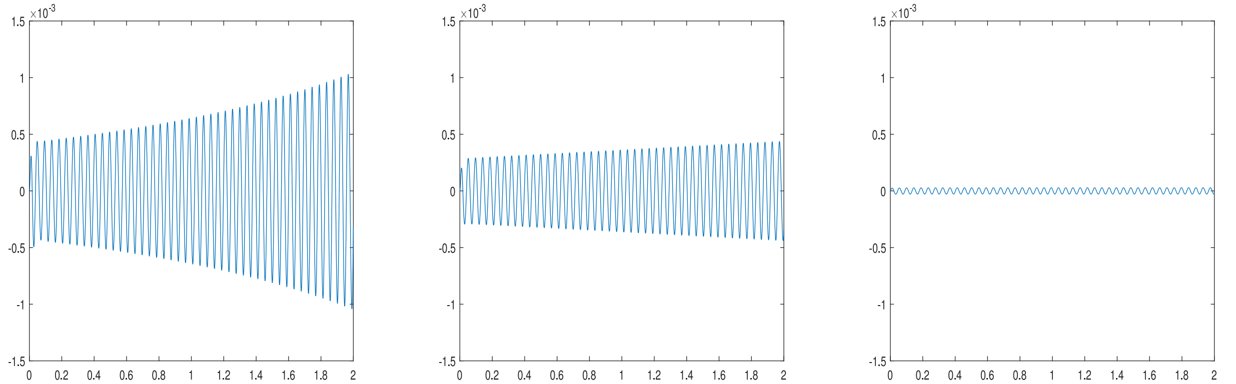

Fig. 8. Left to right: Deflection of the viscoelastic Euler–Bernoulli beam (2.6)–(2.7) on $[0, T]$ with $T = 2\text{s}$ and $\alpha(t) = 0.2 - 0.05t$, $E_d = 0.001E$, $E_d = 0.01E$, and $E_d = 0.2E$, respectively.

about predictions that do not grow linearly in time and generates predictions of vibrations that may agree more with experimental observations [14].

Acknowledgments

The authors would like to express their sincere thanks to the referees for their very helpful comments and suggestions, which greatly improved the quality of this paper. This work was partially supported by the National Science Foundation, United States under Grant No. DMS-201229 and ARO MURI, USA under Grant No. W911NF-15-1-0562.

References

[1] R. Adams, J. Fournier, Sobolev Spaces, Elsevier, San Diego, 2003.
[2] R. Bagley, Power law and fractional calculus model of viscoelasticity, AIAA 27 (1989) 1412–1417.
[3] H. Banks, D. Inman, On damping mechanisms in beams, J. Appl. Mech. 58 (1991) 716–723.
[4] A. Bonfanti, J. Kaplan, G. Charras, A. Kabla, Fractional viscoelastic models for power-law materials, Soft Matter 16 (2020) 6002–6020.
[5] W. Bottega, Engineering Vibrations, second ed., CRC Press, 2013.
[6] R. Christensen, Theory of Viscoelasticity: An Introduction, Academic Press, New York, 1982.
[7] R. Clough, J. Penzien, Dynamics of Structures, John Wiley and Sons, New York, 1975.
[8] M. Di Paola, R. Heuer, A. Pirrotta, Fractional visco-elastic Euler–Bernoulli beam, Int. J. Solids Struct. 50 (2013) 3505–3510.
[9] M. Di Paola, A. Pirrotta, A. Valenza, Visco-elastic behavior through fractional calculus: An easier method for best fitting experimental results, Mech. Mater. 43 (2011) 799–806.
[10] K. Diethelm, The Analysis of Fractional Differential Equations, in: Ser. Lecture Notes in Mathematics, Springer-Verlag, Berlin, 2004.
[11] L. Eldred, W. Baker, A. Palazotto, Kelvin-Voigt versus fractional derivative model as constitutive relations for viscoelastic materials, AIAA J. 33 (1995) 547–550.
[12] L. Evans, Partial Differential Equations, Graduate Studies in Mathematics, Vol. 19, American Mathematical Society, Providence, RI, 1998.
[13] R. Garrappa, A. Giusti, F. Mainardi, Variable-order fractional calculus: a change of perspective, Commun. Nonlinear Sci. Numer. Simul. 102 (2021) 105904.
[14] A. Ghoshal, H. Kim, A. Chattopadhyay, W. Prosser, Effect of delamination on transient history of smart composite plates, Finite Elem. Anal. Des. 41 (2005) 850–874.
[15] P. Hagedorn, G. Spelsberg-Korspeter, Active and passive vibration control of structures, in: CISM International Centre for Mechanical Sciences, in: Courses and Lectures, vol. 558, Springer, Vienna, 2014.
[16] Inconel alloy 718, Publication number SMC-045 copyright special metals corporation, 2007, www.specialmetals.com.
[17] D. Inman, Engineering Vibrations, fourth ed., Pearson, New Jersey, 2014.
[18] A. Jaiseenkar, G. McKinley, Power-law rheology in the bulk and at the interface: quasi-properties and fractional constitutive equations, Proc. R. Soc. Lond. Ser. A Math. Phys. Eng. Sci. 469 (2013) 20120284.
[19] C. Ji, Z. Sun, A high-order compact finite difference scheme for the fractional sub-diffusion equation, J. Sci. Comput. 64 (2015) 959–985.
[20] N. Kopteva, Error analysis of the L1 method on graded and uniform meshes for a fractional-derivative problem in two and three dimensions, Math. Comp. 88 (2019) 2135–2155.

[21] Q. Li, H. Chen, Numerical analysis for compact difference scheme of fractional viscoelastic beam vibration models, Appl. Math. Comput. 427 (2022) 127146.
[22] C. Li, H. Ding, Higher order finite difference method for the reaction and anomalous-diffusion equation, Appl. Math. Model. 38 (2014) 3802–3821.
[23] Y. Li, H. Wang, X. Zheng, A viscoelastic Timoshenko beam model: regularity and numerical approximation, J. Sci. Comput. 95 (2023) 57, http://dx.doi.org/10.1007/s10915-023-02187-5.
[24] G. Lord, C. Powell, T. Shardlow, An Introduction to Computational Stochastic PDEs, Cambridge University Press, 2014.
[25] C. Lorenzo, T. Hartley, Variable order and distributed order fractional operators, Nonlinear Dynam. 29 (2002) 57–98.
[26] F. Mainardi, Fractional Calculus and Waves in Linear Viscoelasticity: An Introduction to Mathematical Models, Imperial College Press, London, 2010.
[27] W. McLean, V. Thomée, Numerical solution of an evolution equation with a positive-type memory term, J. Aust. Math. Soc. Ser. B 35 (1993) 23–70.
[28] W. McLean, V. Thomée, L. Wahlbin, Discretization with variable time steps of an evolution equation with a positive-type memory term, J. Comput. Appl. Math. 69 (1996) 49–69.
[29] M. Meerschaert, A. Sikorskii, Stochastic Models for Fractional Calculus, in: De Gruyter Studies in Mathematics, 2011.
[30] P. Nutting, A new general law deformation, J. Franklin Inst. 191 (1921) 678–685.
[31] I. Podlubny, Fractional Differential Equations, Academic Press, London, 1999.
[32] L. Ramirez, C. Coimbra, A variable order constitutive relation for viscoelasticity, Ann. Physics 519 (2007) 543–552.
[33] S. Rao, Vibration of Continuous Systems, John Wiley Sons, Hoboken, New Jersey, 2019.
[34] J. Reddy, An Introduction to Continuum Mechanics, second ed., Cambridge University Press, New York, 2013.
[35] K. Sakamoto, M. Yamamoto, Initial value/boundary value problems for fractional diffusion-wave equations and applications to some inverse problems, J. Math. Anal. Appl. 382 (2011) 426–447.
[36] S. Samko, B. Ross, Integration and differentiation to a variable fractional order, Integral Transforms Spec. Funct. 1 (1993) 277–300.
[37] M. Stynes, E. O'Riordan, J. Gracia, Error analysis of a finite difference method on graded mesh for a time-fractional diffusion equation, SIAM J. Numer. Anal. 55 (2017) 1057–1079.
[38] H. Sun, A. Chang, Y. Zhang, W. Chen, A review on variable-order fractional differential equations: mathematical foundations, physical models, numerical methods and applications, Fract. Calc. Appl. Anal. 22 (2019) 27–59.
[39] H. Sun, Y. Zhang, W. Chen, D. Reeves, Use of a variable-index fractional-derivative model to capture transient dispersion in heterogeneous media, J. Contam. Hydrol. 157 (2014) 47–58.
[40] H. Sun, X. Zhao, Z. Sun, The temporal second order difference schemes based on the interpolation approximation for the time multi-term fractional wave equation, J. Sci. Comput. 78 (2019) 467–498.
[41] L. Suzuki, E. Kharazmi, P. Varghaei, M. Naghibolhosseini, M. Zayernouri, Anomalous nonlinear dynamics behavior of fractional viscoelastic beams, J. Comput. Nonlinear Dyn. 16 (2021) 111005.
[42] V. Thomée, Galerkin Finite Element Methods for Parabolic Problems, in: Lecture Notes in Math., vol. 1054, Springer-Verlag, New York, 1984.
[43] W. Tian, H. Zhou, W. Deng, A class of second order difference approximations for solving space fractional diffusion equations, Math. Comp. 84 (2015) 1703–1727.
[44] L. Wang, Y. Chen, G. Cheng, T. Barrière, Numerical analysis of fractional partial differential equations applied to polymeric visco-elastic Euler–Bernoulli beam under quasi-static loads, Chaos Solitons Fractals 140 (2020) 110255.
[45] C. Yu, J. Zhang, Y. Chen, Y. Feng, A. Yang, A numerical method for solving fractional-order viscoelastic Euler–Bernoulli beams, Chaos Solitons Fractals 128 (2019) 275–279.
[46] F. Zeng, C. Li, F. Liu, I. Turner, The use of finite difference/element approaches for solving the time-fractional subdiffusion equation, SIAM J. Sci. Comput. 35 (2013) A2976–A3000.
[47] F. Zeng, Z. Zhang, G. Karniadakis, A generalized spectral collocation method with tunable accuracy for variable-order fractional differential equations, SIAM J. Sci. Comput. 37 (2015) A2710–A2732.
[48] X. Zhao, Z. Sun, G. Karniadakis, Second-order approximations for variable order fractional derivatives: algorithms and applications, J. Comput. Phys. 293 (2015) 184–200.
[49] X. Zheng, H. Wang, An error estimate of a numerical approximation to a hidden-memory variable-order space–time fractional diffusion equation, SIAM J. Numer. Anal. 58 (2020) 2492–2514.
[50] X. Zheng, H. Wang, An optimal-order numerical approximation to variable-order space-fractional diffusion equations on uniform or grade meshes, SIAM J. Numer. Anal. 58 (2020) 330–352.
[51] X. Zheng, H. Wang, A hidden-memory variable-order fractional optimal control model: analysis and approximation, SIAM J. Control Optim. 59 (2021) 1851–1880.
[52] P. Zhuang, F. Liu, V. Anh, I. Turner, Numerical methods for the variable-order fractional advection-diffusion equation with a nonlinear source term, SIAM J. Numer. Anal. 47 (2009) 1760–1781.